

1 **Simultaneously assimilating multivariate datasets into the**
2 **two-source evapotranspiration model by Bayesian approach:**
3 **Application to spring maize in an arid region of northwest China**

4 G.F. Zhu¹, X. Li², Y.H. Su², K. Zhang¹, Y. Bai¹, J.Z. Ma¹,
5 C. B. Li¹, **C.L. Huang²**, X. L. Hu², J. H. He¹

- 6
7
8
- 9 1. Key Laboratory of Western China's Environmental Systems (Ministry of
10 Education), Lanzhou University, Lanzhou 730000, China.
 - 11 2. Cold and Arid Regions Environmental and Engineering Research Institute,
12 Chinese Academy of Science, Lanzhou 730000, China.

13
14
15
16 Corresponding Author: Zhu Gaofeng

17 Address: Tianshui Road 222, Lanzhou, Gnasu Province, China, 730000.

18 Email: zhugf@lzu.edu.cn

26 **Abstract**

27 Based on direct measurements of half-hourly canopy evapotranspiration (ET; W m^{-2})
28 using the eddy covariance (EC) system and daily soil evaporation (E ; mm d^{-1}) using
29 microlysimeters over a crop ecosystem in arid northwest China from 27 May to 14
30 Sep. in 2013, a Bayesian method was used to simultaneously parameterize the soil
31 surface and canopy resistances in the Shuttleworth-Wallace (S-W) model. 4 of the six
32 parameters showed relatively larger uncertainty reductions ($>50\%$), and their posterior
33 distributions became approximately symmetric with distinctive modes. There was a
34 moderately good agreement between measured and simulated values of half-hourly
35 ET and daily E with a linear regression being $y=0.84x+0.18$ ($R^2=0.83$) and
36 $y=1.01x+0.01$ ($R^2=0.82$), respectively. The causes of underestimations of ET by the
37 S-W model was possibly attributed to the micro-scale advection, which can contribute
38 an added energy in the form of downward sensible heat fluxes to the ET process.
39 Therefore, the advection process should be taken into account in simulating ET in
40 heterogeneous land surface. Also, underestimations were observed on or shortly after
41 rainy days, which may be due to direct evaporation of liquid water intercepted in the
42 canopy. Thus, the canopy interception model should be coupled to the S-W model in
43 the long-term ET simulation.

44

45 **Keywords:** Bayesian statistics, Crop evapotranspiration, Shuttleworth-Wallace model,
46 Maize, Arid region

47

48 1 Introduction

49 In agriculture ecosystem, more than 90% of all water inputs is lost by
50 evapotranspiration (ET) (Morison et al., 2008), which is defined as the sum of water
51 loss by evaporation (E) from soil and transpiration (T) from plants (Rana and Katerji,
52 2000). E and T are influenced by different abiotic and biotic factors (Wang and Yakir,
53 2000), and the contributions of E and T to the total ecosystem ET are highly variable
54 in space and time (Ferretti et al., 2003). Thus, accurate measurement or estimation of
55 ET and its components (E and T) is essential for many applications in agriculture,
56 such as irrigation scheduling, drainage, and yield forecasts (Wallace and Verhoef,
57 2000; Flumignan et al., 2011; Sun et al., 2012). The Shuttleworth-Wallace model
58 (S-W model) (Shuttleworth and Wallace, 1985) takes the interactions between the
59 fluxes from soil and canopy into account, and is physically sound and rigorous.
60 Previous studies have proved that it performs well for row crops such as maize, wheat,
61 cotton, sorghun and vine (Stannard, 1993; Tourula and Heikinheimo, 1998;
62 Anadranistakis et al., 2000; Teh, et al., 2001; Lund and Soegaard, 2003; Kato et al.,
63 2004; Ortega-Farias et al., 2007; Zhang et al., 2008).

64 Despite these studies, there are still some insufficiencies in the application of the
65 S-W model (Hu et al., 2009; Zhu et al., 2013). First, the S-W model is sensitive to the
66 errors in the values of canopy and soil resistances (Lund and Soegaard, 2003).
67 Previous studies mainly focused on the parameterization of the canopy resistance
68 (Hanan and Prince, 1997; Samanta et al., 2007; Zhu et al., 2013) , and less attentions
69 have been committed to the parameterization of the soil surface resistance (Sellers et

70 al., 1992; van de Griend and Owe, 1994; Villagarcía et al., 2010). In crop ecosystem,
71 E may contribute significantly to the total ET when leaf area index (LAI) is low
72 (Lund and Soegaard, 2003; Zhang et al., 2008). Thus, simultaneous parameterization
73 of the canopy and soil resistances in the S-W model, based on direct measurement of
74 ET and its components by using a combination of micro-meteorological (e.g. eddy
75 covariance methods, Bowen ratio), hydrological (e.g. chambers, microlysimeters) and
76 eco-physiological techniques (e.g. sap-flow, stable isotopes) (Williams et al., 2004;
77 Scott et al., 2006), is important to reduce the model error. However, such studies are
78 relative rare or non-existent. Secondly, as far as the parameterization method is
79 concerned, abundant evidence has shown that the Bayesian method provides a
80 powerful new tool to simultaneously optimize many or all model parameters against
81 all available measurements, and to quantify the influence of uncertainties (Clark and
82 Gelfand, 2006). Although some pioneering efforts have been made (e.g. Samanta et
83 al., 2007; Zhu et al., 2013), the Bayesian method has been much less frequently used
84 in parameterization of ET model than in the other environmental sciences (van Oijen
85 et al., 2005). Moreover, the Bayesian method, to our knowledge, has not been used to
86 simultaneously optimized the parameters of the S-W model against multivariate
87 datasets (section 2.5). Finally, arid northwest China, one of the driest area in the world
88 (Zhu et al., 2007, 2008), is characterized by a widely distributed desert/Gobi
89 interspersed with many oases in different sizes and shapes. Land surface processes of
90 this heterogeneous region are much complex than in other regions (Zhang and Huang,
91 2004). Thus, the applicability of the S-W model in such regions need to be

92 investigated in details.

93 Based on direct measurements of different components of ET obtained by using
94 the eddy covariance technique and microlysimeters over a spring maize field in the
95 arid region of northwest China from 27 May to 14 September in 2013, the objectives
96 of the present study were to: (1) simultaneously parameterize the S-W model using
97 the Bayesian method against **multivariate datasets**; (2) verify the performances of the
98 S-W model, and identify the causes of failure and success in simulating ET over the
99 crop ecosystem in arid desert oasis of northwest China. It is expected that this study
100 can not only promote the developments of ET model parameterization, but also help
101 us to find a proper direction in modifying the S-W model used in arid regions.

102 **2 Materials and methods**

103 **2.1 Study site**

104 The study site is located in Daman (DM) Oasis, in the middle Heihe River Basin,
105 Gansu province, China (100° 22' 20" E, 38° 51' 20" N; 1556 m a. s. l; Fig.1). The
106 annual average temperature and precipitation was 7.2 °C and 125 mm (1960-2000),
107 respectively. The potential evaporation is around 2365 mm year⁻¹, and the dryness
108 index **according to the World Atals of Desertification (UNEP, 1992)** is 15.9. The soil
109 type is silt clay loam on the surface and silt loam in the deeper layer.

110 The study area has an agricultural development history of over 2000 years owing
111 to its flat terrain, adequate sunlight and convenient water resources from Qilian
112 Mountains. The main crops in the DM Oasis are spring wheat and maize. The spring
113 wheat (*Triticum aestivum* L.) is generally sown in the later March and harvested in the

114 middle 10 days of July, while the maize (*Zea mays* L.) is sown in the late April and
115 harvested in the middle 10 days of September. Stand density of the spring maize is
116 about 37 plants m² with row spacing of 40 cm and planting spacing of 7 cm.

117 2.2 Measurements and data processing

118 The field observation systems at this site were constructed in May 2013 as part
119 of the Heihe Watershed Allied Telemetry Experimental Research (HiWATER) project
120 (See details in Li et al., 2013b). The fluxes of sensible heat (H), latent heat (λET) and
121 carbon dioxide were measured at the height 4.5 m using the eddy covariance (EC)
122 system (Liu et al., 2013, manuscript in preparation), which consists of an open-path
123 infrared gas analyzer (Li-7500, LiCor Inc., Lincoln, NE, USA) and a 3D sonic
124 anemometer (CSAT-3, Campbell Scientific Inc., Logan, UT, USA). The EC data were
125 sampled at a frequency of 10 Hz by a data logger (CR5000, Campbell Scientific Inc.),
126 and then were processed with an average time of 30 min. Post-processing calculations,
127 using EdiRe software, included spike detection, lag correction of H₂O/CO₂ relative to
128 the vertical wind component, sonic virtual temperature conversion, planar fit
129 coordinate rotation, the WPL density fluctuation correction and frequency response
130 correction (Xu et al., 2014). About 85% energy balance closure (the sum of $H+\lambda ET$
131 against the available energy) was found in EC data (Liu et al., 2011). In addition, the
132 flux uncertainties are directly related to the likelihood function of Bayesian inference
133 (Section 2.5). Thus, determining the uncertainties in EC measurements is essential for
134 proper parameter estimates. Recently, Wang et al. (2014) systemically studies the flux
135 uncertainties of EC systems equipped in the HiWATER experiment. Generally,

136 uncertainties for H ($\sigma_r(H)$; W m^{-2}) by using method of Mann and Lenschow (1994)
137 tended to be $\sigma_r(H) = 0.14H + 2.7$ ($R^2=0.95$), and uncertainties for λET ($\sigma_r(\lambda ET)$;
138 W m^{-2}) be $\sigma_r(\lambda ET) = 0.13\lambda ET + 6$ ($R^2=0.93$) (Wang et al., 2014). Data gaps due to
139 instrument malfunction, power failure and bad weather conditions were filled using
140 artificial neural network (ANN) and mean diurnal variations (MDV) methods (Falge
141 et al., 2001). The ANN method was applied when the synchronous meteorological
142 data were available; otherwise, the MDV method was used. The gap-filling data were
143 used only to analyze the seasonal and annual variations in ET.

144 Continuous complementary measurements also included standard
145 hydro-meteorological variables. Rainfall was measuring using a tipping bucket rain
146 gauge (TE525MM, Campbell Scientific Instruments Inc.). Air temperature, relative
147 humidity (HMP45C, Vaisala Inc., Helsinki, Finland) and wind speed/direction (034B,
148 Met One Instruments, Inc. USA) were measured at heights of 3, 5, 10 15, 20, 30 and
149 40 m above the ground. Downward and upward solar and longwave radiation (PSP,
150 The EPPLEY Laboratory Inc., USA) and photosynthetic photon flux density (PPFD)
151 (LI-190SA, LI-COR Inc.) were measured at height of 6 m. Soil temperature
152 (Campbell-107, Campbell Scientific Instruments Inc.) and moisture (CS616,
153 Campbell Scientific Instruments Inc.) was measured at 0.02, 0.04, 0.1, 0.2, 0.4, 0.8,
154 1.2 and 1.6 m depths. Three heat flux plates (HFT3, Campbell Scientific Instruments
155 Inc.) were randomly buried at the depths of 0.01 m. The average soil heat fluxes
156 were calculated using the three randomly buried plates. These data were logged every
157 10 min by a digital micrologger (CR23X, Campbell Scientific Inc.) equipped with an

158 analog multiplexer (AM416) used for sampling and logging data.

159 Daily soil evaporation was measured using three microlysimeters randomly
160 placed between crop rows (one in the middle of the rows and the other two close to
161 plants on each side of the rows). The microlysimeters with an internal diameter of 10
162 cm and a depth of 20 cm were filled with an intact soil core and pushed into soil with
163 the top slightly above the soil surface (Daamen et al., 1993; Liu et al., 2002). The
164 average weight loss of these microlysimeters measured using electronic scales with
165 0.01 g precision was nearly equal to soil evaporation. In order to keep the soil
166 moisture in microlysimeters similar to that between the rows, the soil in the
167 microlysimeters was replaced daily or every two days.

168 Leaf area index (LAI) was measured using AM300 portable leaf area meter
169 (ADC BioScientific Ltd., UK). The fraction of land cover (f) was estimated by
170 measuring the projected crop canopy area of selected stands in corresponding field
171 plot. LAI, f and crop height were measured approximately every 10 days during
172 the growing season, and the gaps were linearly interpolated to daily interval.

173 2.3 Description of the S-W model

174 In the S-W model, the ecosystem evapotranspiration (λET ; $W m^{-2}$) is separated
175 into evaporation from the soil surface (λE ; $W m^{-2}$) and transpiration from the
176 vegetation canopy (λT ; $W m^{-2}$) (Fig. 2), which are calculated as (Shuttleworth and
177 Wallace, 1985; Lhomme et al., 2012):

$$178 \lambda ET = \lambda E + \lambda T = C_s ET_s + C_c ET_c \quad (1)$$

$$179 ET_s = \frac{\Delta A + [\rho C_p D - \Delta r_a^s (A - A_s)] / (r_a^a + r_a^s)}{\Delta + \gamma [1 + r_s^s / (r_a^a + r_a^s)]} \quad (2)$$

$$180 \quad ET_c = \frac{\Delta A + [\rho C_p D - \Delta r_a^c A_s] / (r_a^a + r_a^c)}{\Delta + \gamma [1 + r_s^c / (r_a^a + r_a^c)]} \quad (3)$$

$$181 \quad C_s = \frac{1}{1 + [R_s R_a / R_c (R_s + R_a)]} \quad (4)$$

$$182 \quad C_c = \frac{1}{1 + [R_c R_a / R_s (R_c + R_a)]} \quad (5)$$

$$183 \quad R_a = (\Delta + \gamma) r_a^a \quad (6)$$

$$184 \quad R_c = (\Delta + \gamma) r_a^c + \gamma r_s^c \quad (7)$$

$$185 \quad R_s = (\Delta + \gamma) r_a^s + \gamma r_s^s \quad (8)$$

$$186 \quad \lambda E = \frac{\Delta A_s + \rho C_p D_0 / r_a^s}{\Delta + \gamma (1 + r_s^s / r_a^s)} \quad (9)$$

$$187 \quad \lambda T = \frac{\Delta (A - A_s) + \rho C_p D_0 / r_a^c}{\Delta + \gamma (1 + r_s^c / r_a^c)} \quad (10)$$

$$188 \quad D_0 = D + \frac{(\Delta A - (\Delta + \gamma) \lambda ET) r_a^a}{\rho C_p} \quad (11)$$

189 where ET_s and ET_c are terms to describe evaporation from soil and transpiration
190 from the plant ($W m^{-2}$), respectively; C_s and C_c are soil surface resistance and
191 canopy resistance **coefficients** (dimensionless), respectively; λ is the latent heat of
192 evaporation ($J kg^{-1}$); Δ is the slope of the saturation vapor pressure versus
193 temperature curve ($kPa K^{-1}$); ρ is the air density ($kg m^{-3}$); C_p is the specific heat
194 capacity of dry air ($1013 J kg^{-1} K^{-1}$); D and D_0 (kPa) **are** the air water vapor
195 pressure deficit at the reference height (3 m) and the canopy height, respectively; γ is
196 the psychrometric constant ($kPa K^{-1}$); r_s^c and r_s^s are the surface resistance for plant
197 canopy and soil surface ($s m^{-1}$), respectively; r_a^c and r_a^s are aerodynamic resistances
198 from the leaf to canopy height and soil surface to canopy height ($s m^{-1}$), and r_a^a is

199 aerodynamic resistances from canopy height to reference height ($s\ m^{-1}$). A and A_s
200 ($W\ m^{-2}$) are the available energy input above the canopy and above the soil surface,
201 respectively, and are calculated as:

$$202 \quad A = R_n - G \quad (12)$$

$$203 \quad A_s = R_{ns} - G \quad (13)$$

204 where R_n and R_{ns} are net radiation fluxes into the canopy and the substrate ($W\ m^{-2}$),
205 respectively; G is the soil heat flux ($W\ m^{-2}$). R_{ns} was calculated using a Beer's law
206 relationship of the form:

$$207 \quad R_{ns} = R_n \exp(-K_A LAI) \quad (14)$$

208 in which K_A is the extinction coefficient of light attenuation. It **can be measured on**
209 **site (see Sauer et al., 2007), and was set to be** approximately 0.41 for spring maize
210 **(Mo et al., 2000).**

211 The climate-related variables (i.e., λ , e_s , Δ , ρ and γ) in Eqns. (1)-(3) **are**
212 **calculated by the formulas of Allen et al. (1998).**

213 **2.4 Calculation of resistances in the S-W model**

214 The resistance network of the S-W model is shown in Fig. 2. In this paper, the
215 three aerodynamic resistance (i.e., r_a^a , r_a^c and r_a^s) were calculated using the same
216 approach suggested by Shuttleworth and Wallace (1985), Shuttleworth and Gurney
217 (1990) and Lhomme et al. (2012).

218 The canopy resistance (r_s^c), which is the equivalent resistance of all the
219 individual stomates in a canopy and depends on the environmental variables, can be
220 calculated using the Jarvis-type model (Jarvis, 1976)

$$221 \quad r_s^c = \frac{r_{STmin}}{2LAI \prod_i F_i(X_i)} \quad (15)$$

222 where r_{STmin} represents the minimal stomatal resistance of individual leaves under
 223 optimal conditions. $F_i(X_i)$ is the stress function of a specific environmental variable
 224 X_i , with $0 \leq F_i(X_i) \leq 1$. Following Stewart (1998) and Verhoef and Allen (2000), the
 225 stress functions were expressed as:

$$226 \quad F_1(R_s) = \frac{R_s}{1000} \frac{1000 + k_1}{R_s + k_1} \quad (16)$$

$$227 \quad F_2(T_a) = \frac{(T_a - T_{a,min})(T_{a,max} - T_a)^{(T_{a,max} - k_2)/(k_2 - T_{a,min})}}{(k_2 - T_{a,min})(T_{a,max} - k_2)^{(T_{a,max} - k_2)/(k_2 - T_{a,min})}} \quad (17)$$

$$228 \quad F_3(D) = 1 - k_3 D \quad (18)$$

$$229 \quad F_4(\theta_r) = \begin{cases} 1 & \theta_r > \theta_{cr} \\ \frac{(\theta_r - \theta_{wp})}{(\theta_{cr} - \theta_{wp})} & \theta_{wp} \leq \theta_r \leq \theta_{cr} \\ 0 & \theta_r < \theta_{wp} \end{cases} \quad (19)$$

230 where $k_1 - k_3$ are constants (units see Table 1); R_s is the incoming solar radiation
 231 (W m^{-2}); T_a is the air temperature ($^{\circ}\text{C}$) at the reference height; $T_{a,min}$ and $T_{a,max}$ are
 232 the lower and upper temperatures limits ($^{\circ}\text{C}$), respectively, which are T_a values when
 233 $F_2(T_a) = 0$ and are set at values of 0 and 40 $^{\circ}\text{C}$ (Harris et al., 2004); θ_r is the actual
 234 volumetric soil water content in the root-zone at depth of 0-60 cm ($\text{m}^3 \text{m}^{-3}$); θ_{wp} is
 235 water content at the wilting point ($\text{m}^3 \text{m}^{-3}$); and θ_{cr} is the critical water content (m^3
 236 m^{-3}) at which plant stress starts. **The values of θ_{wp} and θ_{cr} are set as 0.11 $\text{m}^3 \text{m}^{-3}$**
 237 **and 0.30 $\text{m}^3 \text{m}^{-3}$ for sandy loam in the study area (Zhao et al., 2010).**

238 The soil surface resistances (r_s^s ; Fig. 2) was expressed as a function of
 239 near-surface soil water content (Sellers, 1992; Verhoef et al., 2006, 2012; Zhu et al.,

240 2013):

$$241 \quad r_s^s = \exp(b_1 - b_2 \frac{\theta_s}{\theta_{\text{sat}}}) \quad (20)$$

242 in which b_1 and b_2 are empirical constants (s m^{-1}); θ_s is soil water content in the
243 top layer of soil (at depth of 2cm); θ_{sat} is the saturated soil water content ($\text{m}^3 \text{ m}^{-3}$),
244 which was estimated empirically through the near-surface soil texture. In summary,
245 there are 6 site- and species-specific parameters that needed to be estimated in the
246 S-W model associated with soil and canopy resistances, which are b_1 , b_2 , r_{STmin} and
247 $k_1 - k_3$ (see Appendix A).

248 **2.5 Bayesian inference framework and assimilation scheme**

249 With Bayes' theorem (a complete description was presented in Appendix B), the
250 posterior distribution of parameters \mathbf{c} is generated by:

$$251 \quad p(\mathbf{c} | \mathbf{O}) \propto p(\mathbf{O} | \mathbf{c}) p(\mathbf{c}) \quad (21)$$

252 where $p(\mathbf{c})$ represents prior probability distributions of parameters \mathbf{c} , which is chosen
253 as uniform distributions with specified allowable ranges (Table 1). In general, the
254 parameter ranges were wide enough to include the actual parameter values and to give
255 the optimization freedom (Sack et al., 2006). In the test study, we run the S-W model
256 using 4000 parameter vectors which were sampled from the prior distribution using
257 Latin Hypercube Sampling (LHS) method (Iman and Helton, 1998), and found that
258 the observed data in most case were in the range of predicted values (Appendix A);

259 $p(\mathbf{O} | \mathbf{c})$ is the likelihood function, which reflects the influence of the observation
260 datasets on parameter identification; and $p(\mathbf{c} | \mathbf{O})$ is the posterior distribution after
261 Bayesian inference conditioned on available observations \mathbf{O} .

262 For each dataset (e.g., λ ET and E), the model-data mismatch $e_i(t)$ ($i=1,2$),
 263 which represents a relative “goodness-of-fit” measure for each possible parameter
 264 vector (van Oijen et al., 2011, 2013), is expressed by:

$$265 \quad e_i(t) = O_i(t) - f_i(t) \quad (22)$$

266 where $O_i(t)$ and $f_i(t)$ are observed and modeled (equations (1) or (9)) values of the
 267 i th dataset at time t , respectively. Assuming the model-data mismatch $e_i(t)$ follows a
 268 Gaussian distribution with a zero mean, the likelihood function for the i th dataset
 269 ($\mathbf{O}_i(\cdot)$) can be expressed by:

$$270 \quad p(\mathbf{O}_i(\cdot) | \mathbf{c}) = \prod_{t=1}^{n_i} \frac{1}{\sqrt{2\pi}\sigma_i} e^{-\frac{(e_i(t))^2}{2\sigma_i^2}} \quad (23)$$

271 where n_i is the number of observations of the i th dataset; σ_i ($i=1,2$) represents
 272 the residual errors, or standard deviation about model predicted output of the i th
 273 dataset. Here, we assumed σ_i is the same over the observation time for the i th
 274 dataset (Braswell et al., 2005). Traditionally, σ_i can be included into the analysis
 275 explicitly (i.e., assuming σ_i is uniform over $\log \sigma_i$; Gelman et al., 1995) and treated
 276 as one the model parameters, which yields a complete posterior distribution of σ_i .
 277 However, this method artificially increased the parameter dimension of the problem
 278 and may result in unreasonable estimations of the parameter values (Kavetski et al.,
 279 2006). In this study, σ_i was estimated by using the analytical method (Hurtt and
 280 Armstrong, 1996; Braswell et al., 2005), which is to find the value of σ_i that
 281 maximizes $\log(p(\mathbf{O}_i(\cdot) | \mathbf{c}))$ for a given parameter vector. By differentiating
 282 $\log(p(\mathbf{O}_i(\cdot) | \mathbf{c}))$ with respect to σ_i , we can obtain:

283
$$\sigma_i^a = \sqrt{\frac{1}{n_i} \sum_{t=1}^{n_i} (e_i(t))^2}$$
 (24)

284 We then used σ_i^a to replace σ_i in the equations (22).

285 The likelihood function for the **multivariate datasets**, $p(\mathbf{c} | \mathbf{O})$, used for
 286 parameter estimation is then defined as the product of the individual $p(\mathbf{O}_i(\cdot) | \mathbf{c})$'s
 287 (Richardson et al., 2010):

288
$$p(\mathbf{O} | \mathbf{c}) = \prod_{i=1}^m p(\mathbf{O}_i(\cdot) | \mathbf{c}) = \prod_{i=1}^m \prod_{t=1}^{n_i} \frac{1}{\sqrt{2\pi}\sigma_i} e^{-\frac{(e_i(t))^2}{2\sigma_i^2}}$$
 (25)

289 where m is the number of dataset; **When a particular dataset $\mathbf{O}_i(\cdot)$ was not being**
 290 **used in the optimization, we simply set the corresponding likelihood function**
 291 **$p(\mathbf{O}_i(\cdot) | \mathbf{c})$ to 1. Thus, this framework can be easily used when additional**
 292 **observations are available.** In this studies, the two **datasets** used to simultaneously
 293 optimize the parameter values were: EC-measured half-hourly evapotranspiration
 294 (λET ; Wm^{-2}) and microlysimeters-measured daily soil evaporation (E ; mm d^{-1}).

295 **2.6 Metropolis-Hasting algorithm and convergence test**

296 The posterior distribution was sampled using the Metropolis–Hasting (M-H)
 297 algorithm (Metropolis et al., 1953; Hastings, 1970), a version of the Markov Chain
 298 Monte Carlo (MCMC) technique. To generate a Markov chain in the parameter space,
 299 the M-H algorithm was run by repeating two steps: a proposing step and a moving
 300 step. In the proposing step, a candidate point \mathbf{c}^{new} is generated according to a
 301 proposal distribution $P(\mathbf{c}^{\text{new}} | \mathbf{c}^{k-1})$, where \mathbf{c}^{k-1} is the accepted point at the previous
 302 step. In the moving step, point \mathbf{c}^{new} is treated against the Metropolis criterion to
 303 examine if it should be accepted or rejected. **It was well recognized that efficiency of**

304 the M-H algorithm was strongly effected by the proposal distribution function. To find
305 an effective proposal distribution $P(\mathbf{c}^{\text{new}} | \mathbf{c}^{k-1})$, a test run of the M-H algorithm with
306 10, 000 simulations was made by using a uniform proposal distribution (Braswell et
307 al., 2005):

$$308 \quad \mathbf{c}^{\text{new}} = \mathbf{c}^{k-1} + r(\mathbf{c}^{\text{max}} - \mathbf{c}^{\text{min}}) \quad (26)$$

309 where \mathbf{c}^{k-1} is the current accepted point; r is a random number uniformly
310 distributed between -0.5 and +0.5; \mathbf{c}^{min} and \mathbf{c}^{max} are the lower and upper limits of
311 parameter vector \mathbf{c} (Table 1). Based on the test run, we then constructed a normal
312 proposal distribution $\mathbf{c}^{\text{new}} : N(\mathbf{c}^{(k-1)}, \text{cov}^0(\mathbf{c}))$, where $\text{cov}^0(\mathbf{c})$ is the covariance
313 matrix of the parameter vector \mathbf{c} from the initial test run (Xu et al., 2006). The
314 detailed description on MCMC sampling procedure and the code written in Matlab
315 were presented in Appendix B.

316 We ran at least four parallel MCMC chains with 20,000 iterations each,
317 evaluated the chain convergence using the Gelman-Rubin (G-R) diagnostic method
318 (Gelman and Rubin, 1992) (Appendix C), and thinned the chains (every 20th iteration)
319 when appropriate to reduce within chain autocorrelation, thereby producing an
320 independent sample of 3000 values for each parameter from the joint posterior
321 distribution.

322 **2.6 Evaluation of model output estimates**

323 Since the primary interest in application of the S-W model was to reproduce the
324 pattern of water vapour fluxes from different sources (i.e., soil and vegetation) during
325 the whole study period, we used all available data to construct the likelihood function

326 (equation 25) and to obtain the posterior distribution of the parameters. Then, the
 327 performance of the S-W model was evaluated using the coefficient of determination
 328 of the linear regression between measured and estimated values of water vapor
 329 fluxes, R^2 , representing how much the variation in the observations was explained by
 330 the models. Also, the root mean square error (RMSE), mean bias error (MBE), index
 331 of agreement (IA) and model efficiency (EF) (Legates and McCabe, 1999;
 332 Poblete-Echeverria & Ortega-Farias, 2009) were included in the statistical analysis,
 333 which are calculated as follows:

$$334 \quad \text{RMSE} = \sqrt{\frac{1}{n_i} \sum_{t=1}^{n_i} [O_i(t) - f_i(t)]^2} \quad (26)$$

$$335 \quad \text{MBE} = \frac{1}{n_i} \sum_{t=1}^{n_i} [O_i(t) - f_i(t)] \quad (27)$$

$$336 \quad \text{IA} = 1 - \frac{\sum_{t=1}^{n_i} [O_i(t) - f_i(t)]^2}{\sum_{t=1}^{n_i} [|O_i(t) - \bar{O}_i| + |f_i(t) - \bar{O}_i|]^2} \quad (28)$$

$$337 \quad \text{EF} = 1 - \frac{\sum_{t=1}^{n_i} [O_i(t) - f_i(t)]^2}{\sum_{t=1}^{n_i} [O_i(t) - \bar{O}_i]^2} \quad (29)$$

338 where n_i is the total number of observations of the i th dataset; $O_i(t)$ is the observed
 339 values at time t of the i th dataset, \bar{O}_i is the mean of the observed value of the i th
 340 dataset, and $f_i(t)$ is the simulation which was calculated using the posterior median
 341 parameter values, and other parameter vectors selected from the parameter chains
 342 generated by the MCMC iteration (van Oijen et al., 2013).

343 **3 Results**

344 **3.1 Environmental and biological factors**

345 Detailed information on the seasonality of key environmental and biological
346 variables is essential to assess seasonal variation in the actual ET and its partitioning.
347 The seasonal change in net solar radiation (R_n ; MJ m⁻² d⁻¹), air temperature (T_a ; °C),
348 air water vapor pressure deficit (D ; kPa), wind speed (u , m s⁻¹) at the height of 3 m,
349 rainfall and irrigation (mm), soil water content (θ ; m³ m⁻³), and leaf area index (LAI;
350 m² m⁻²) are illustrated in Fig. 3. During the study period (DOY147-257), the daily
351 mean R_n varied from 2.6 to 18.5 MJ m⁻² d⁻¹ with an average value of 11.9 MJ m⁻² d⁻¹.
352 The peaked values were recorded from the end of June to the middle of July
353 (DOY180-195). The variation of mean daily air temperature (T_a) has a similar trend
354 to R_n , varying from 8.8 to 24.9 °C with an average value of around 19.0 °C. D
355 exhibited large diurnal variation ranging from 0 to 3.5 kPa, and the daily mean D was
356 relative small when the LAI was larger than 3 m² m⁻² (DOY197-230). Daily mean
357 wind speed (u) ranged from 0.5 to 3.2 m s⁻¹, and was close to normal long-term
358 values. Total precipitation during the study period was 104.2 mm with eight events
359 over 5.0 mm (Fig. 3). θ varied greatly over the whole growing season. The
360 variability of θ mainly depended on irrigation scheduling of local government
361 (irrigation quota and timing). Soil water content had a peak value (about 0.35 m³ m⁻³)
362 after irrigation and gradually reduced till the next irrigation (Fig. 3). The LAI showed
363 a clear ‘one peak’ pattern over the whole growing season with relative high values of
364 3.5 m² m⁻² from early July to late August (DOY184-221).

365 **3.2 Posterior distribution of S-W model parameters**

366 The posterior parameter distributions are shown as histograms in Fig. 4 and
367 summarized in Table 1 by posterior medians and 95% probability intervals. The
368 results showed that the Bayesian calibration against the multivariate datasets was in
369 most cases successful in reducing the assumed prior ranges of the parameters values.
370 Parameters r_{STmin} , b_1 , b_2 and k_2 showed relatively large uncertainty reductions
371 (defined as $1 - CI_{posterior} / CI_{prior}$, where CI is the length of the 95% credible interval)
372 (Fig. 5), and their posterior distributions became approximately symmetric with
373 distinctive modes, while parameters k_1 and k_3 have relative large variability
374 (widely spread on the prior bounds) (Fig. 4). The global sensitivity analysis with the
375 first-order impact ratio (FOIR) values (Appendix A) reveals the importance of input
376 parameters in affecting total ecosystem evapotranspiration. The results indicated that
377 total ET responded sensitively to r_{STmin} , b_1 , b_2 and k_2 with FOIR values being
378 54.3%, 21.9%, 10.4% and 8.5% (Appendix A), respectively. Other parameters
379 exhibits relative low (<5%) FOIR values, suggesting that the variability in these
380 parameters had almost no effect on the variability in model output. It is worth noting
381 that the four highest sensitive parameters (r_{STmin} , b_1 , b_2 and k_2) also corresponded
382 to the greatest degree of updating in the Bayesian inference. Thus, we thought that the
383 key parameters in the S-W model were well optimized by the Bayesian method
384 against the multivariate datasets. In addition, the correlation coefficient between the
385 posterior distribution of parameters can be used to find groups of parameters tend to
386 be constrained together (Knorr and Kattge, 2005). In this study, the six calibrated
387 parameters were not significantly inter-correlated with each other with correlation

388 coefficients lower than 0.1 (Appendix B).

389 The responses of soil surface resistances (r_s^s) to soil water content computed
390 using our posterior mean b_1 and b_2 values were very similar to that calculated using
391 equation developed by Ortega-Farias et al. (2010) based on direct soil evaporation
392 measurements, but seemed to be more sensitive to changes in soil water content
393 compared with some other studies (e.g., Sun, 1982; Sellers, 1992; Zhu et al., 2013;
394 Fig. 6). When just using EC-measured λET data, a relative wider posterior distribution
395 of b_2 was observed (see Appendix B). Thus, the daily soil evaporation data helped to
396 well constrain estimates of b_1 and b_2 . The posterior mean value of r_{STmin} from our
397 study was very close to that (20 s m^{-1}) reported for spring maize growing in
398 northwest China obtained by using the least squares fitting method (Li et al., 2013a).
399 The variations of the minimal stomatal resistance (r_{STmin}) for many natural and
400 cultivated plants have been widely investigated by previous studies (Korner et al.,
401 1979; Pospisilova and Solarova, 1980). Typical values for r_{STmin} vary considerably
402 from about 20-100 s m^{-1} for crops to 200-300 s m^{-1} for many types of trees. Thus, our
403 results fell within the range of previous studies. However, some parameters related to
404 canopy surface resistance (i.e., k_1 and k_3) seemed to be not well updated (Fig. 4). This
405 may be due to the fact that these parameters may be insensitive to the present
406 available datasets.

407 3.3 Model performance compared with measurements

408 Having parameterized the S-W model as described above, we ran the model to
409 simulate the half-hourly λET (equation 1) and λE (equation 9) values (W m^{-2}). The

410 daily estimations of evapotranspiration (ET; mm d⁻¹) and soil evaporation (E ; mm d⁻¹)
411 were obtained by summing up the half-hourly simulated values. The statistical
412 analysis of observed versus estimated values of water vapor fluxes at different
413 time-scales are summarized in Table 2. These results indicated that the parameterized
414 S-W model was able to predict λ ET on a half-hourly basis with values of R^2 , IA and
415 EF equal to 0.83, 0.93 and 0.74, respectively. However, significant differences exist
416 between measured and modeled half-hourly λ ET values for the spring maize in the
417 arid desert oasis. The slope (0.84) of regression equation between the measured and
418 modeled half-hourly λ ET values was lower than one (Table 2 and Fig. 7a), which
419 indicated that the S-W model tended to underestimate the half-hourly λ ET with a
420 MBE value of 24.2 W m⁻². Ortega-Farias et al. (2010) also reported that the S-W
421 model underestimated on half-hourly time intervals compared the EC-measured λ ET
422 over a drip-irrigated vineyard in Mediterranean semiarid region during the growing
423 season in 2006. On the contrary, some studies showed that the S-W model
424 overestimated half-hourly λ ET (e.g., Li et al., 2013a; Ortega-Farias et al., 2007;
425 Zhang et al., 2008). Therefore, the performances of the S-W model seemed to be
426 variable for different crops and places, and there is a need to identify the causes that
427 induced the disagreements between observed and modeled values (discussed below).

428 The fluctuation of measured and estimated daily ET and E is illustrated in Fig. 8.
429 In this case, a good agreement between measured and estimated daily E was obtained
430 with values of R^2 , IA and EF equal to 0.82, 0.94 and 0.76 (Table 2). The points in
431 plots of measured-versus-modeled daily E fell tightly along the 1:1 line (slope=1.01

432 and intercept=0.01 with RMSE=0.05 and MBE=-0.01; Fig. 7b and Table 2). Also, the
433 95% posterior prediction intervals of simulated soil E was narrow. Thus, we thought
434 that the soil resistance in the S-W model was properly parameterized for the spring
435 maize by the measured soil evaporation data. From Fig. 8, we can also observe that
436 the estimated daily ET generally fluctuated tightly with the measured values with
437 relative narrow uncertainties (95% posterior prediction intervals). The values of
438 RMSE, MBE, IA and EF were equal to 0.05, 0.14 mm d⁻¹, 0.94 and 0.79, respectively
439 (Table 2). However, there are 12 days during the study period (111 days) with
440 observations beyond the upper bounder of the 95% posterior prediction intervals (Fig.
441 8). For example, on the 5th of July, the estimated using the median values of the
442 parameters and measured daily ETs were 2.9 and 4.3 mm d⁻¹, respectively (Fig. 8).
443 Thus, the causes of the underestimations of ET by the S-W on these days needs to be
444 carefully checked based on detailed micrometeorological data. This work would help
445 us to modify the model in a correct way and improve the precision of prediction.

446 **3.4 Identification of the disagreement/agreement between observed and modeled** 447 **ET values**

448 The diurnal variation of R_n , H and λET (measured and modeled) above the
449 spring maize ecosystem for some selected days is presented in Fig. 9. The
450 uncertainties of H and λET increased with the flux magnitude (Fig. 9), and tended
451 to be approximately 14% and 13%, respectively (Wang et al., 2014). The relative error
452 for R_n was relatively small and estimated to be 1.24% (Xu et al., 2013). Resulting
453 from the high surface heterogeneities, one special phenomenon, known as the “oasis

454 effect” (Lemon et al., 1957; Oke, 1978) or “cold island effect” (Wang et al., 1992;
455 Zhang and Huang, 2004), was often observed on clear days in July and August in the
456 study area and it is characterized as follows: (1) H is very small and even negative
457 (downward) in the afternoon (Figs. 9a-c) due to the micro-scale advection of hot dry
458 air over the desert to crop surface in the oasis (Oke, 1978; Hu et al., 1994). For an
459 example, on the 5th of July, H was continuously negative from 12 : 00 to 20 : 00 (Fig.
460 9a). A strong advection process can be distinctly detected from the temperature and
461 relative humidity profiles (Figs. 10a and 10b), in which the highest temperature
462 occurred at a height of 8-18 m; (2) measured actual λET often exceeded (Fig. 9a) or
463 was equal to (Figs. 9b and 9c) the local net radiation because of the added energy in
464 the form of downward fluxes of H to the ET process (Evelt et al., 2012). Under such
465 conditions, the S-W model significantly underestimated the actual ET values due to
466 the real atmospheric flows that do not correspond to its assumption of horizontal
467 homogeneities (Rao et al., 1974). Thus, how to properly represent the advection
468 process in the S-W model should be paid special attention in simulating ET over crop
469 ecosystems in arid desert oasis in the future studies. In addition to this situation, slight
470 underestimations were also observed on or shortly after rainy days (Fig. 8). For
471 example, the simulated half-hourly λET was lower than that measured by EC after the
472 rainfall event occurred in 13 : 00 on 17 June (Fig. 9d). We thought that the
473 underestimations by the model on or shortly after rainy days were mainly due to
474 ignoring the direct evaporation of liquid water intercepted in the crop canopy, because
475 no downward H and temperature inversion were observed on this day (Figs. 10c and

476 10d). Until now, several canopy interception models have been developed (e.g., [Rutter](#)
477 [et al., 1971](#); [Mulder, 1985](#); [Gash et al., 1995](#); [Bouten et al., 1996](#)). However, many of
478 them were developed for simulating the rainfall interception by forest ecosystems, and
479 their suitability for crops need to be further investigated.

480 The diurnal variation of simulated half-hourly λ ET by the parameterized S-W
481 model has a similar trend to the measurements on clear and advection-absent days
482 during the whole study periods (Figs. 9e-h). On these days, H was positive (upwards)
483 at day time (Figs. 9e-h) and no temperature inversion was observed (Figs. 10e and
484 10f). Thus, we thought that the parameterization schedule adopted in this study
485 worked well. It also demonstrated that the properly parameterized S-W model can be
486 used in simulating and partitioning ET for homogeneous land surface. [Hu et al. \(2009\)](#)
487 reported that the S-W model parameterized by using Monte Carlo method can
488 successfully simulated ET at four uniform grasslands in China; Our previous studies
489 ([Zhu et al., 2013](#)) also illustrated that parameterized S-W model can be used to
490 simulate and partition ET over a vast alpine grassland in Qinghai-Tibet Plateau.

491 **4 Discussion**

492 The assessment of model errors remains an outstanding challenge in Hydrology
493 ([Beven, 2008](#)). Identifying the uncertainties related to model parameter and structure
494 needs to take on a prominent position in the hydrological modeling ([Bastola et al.,](#)
495 [2011](#); [Brigode et al., 2013](#)). An important issue in identifying the parameter
496 uncertainty is equifinality, where different parameters of the same model yield similar
497 results, and so can be difficult to distinguish which is correct (see [Franks et al., 1997](#)).

498 A variety of recent studies corroborated the multi-objective calibration against the
499 multiple (orthogonal; see Winsemius et al., 2006) datasets can produce a robust
500 parameter estimates (e.g., Engeland et al., 2006; Fenicia et al., 2007; Moussa and
501 Chahinian, 2009; Richardson et al., 2010; Hrachowitz et al., 2013). In this study, we
502 constructed a Bayesian inference framework to constrain the model parameters using
503 the EC-measured ET and microlysimeters-measured daily E datasets simultaneously.
504 The results indicated that 4 of the six main parameters were considerably updated, and
505 simulated λET and E were comparable to the measurements with relatively narrow
506 uncertainties (95% posterior predication intervals). Using just EC-measured ET data
507 in our test study (see Appendix B), the optimized S-W model on the simulations of
508 λET were not significantly different from that optimized by multivariate datasets
509 procedure, but it significantly underestimated E with great uncertainties (Appendix B).
510 Thus, we can not ensure the S-W model optimized using only the EC-measured ET
511 data can properly partition the total ET into its different components (soil evaporation
512 and plant transpiration), even though the simulated λET values were in good
513 agreement with measurements. Limited success in estimating process-based model
514 parameters using EC-measured data alone were also reported in previous studies (e.g.,
515 Wang et al., 2001; Knorr and Kattge, 2005; Richardson et al., 2010).

516 With the developments of observation technologies and strategies, major steps
517 forwards have been made in extracting a wide variety of environmental data
518 (Hrachowitz et al., 2013). Thus, it is critical to assess to what extent the uncertainty in
519 model parameters and model predictions is reduced by the use of additional data and

520 what new observation is required. The Bayesian inference framework used in this
521 study provided a convenient way to simultaneously constrain model parameters when
522 the new observation datasets are available. However, even with all datasets
523 (EC-measured λ ET and microlysimeters-measured daily E), some parameters related
524 to canopy surface resistance seemed to be not well updated (Fig. 4). We thought that
525 this may be due to the insensitivities of these parameters (e.g., k_1 , k_3 , T_{amax} , T_{amin} and
526 K_A) to the present available datasets. Thus, direct observations of plant transpiration
527 using sap flow or stable isotope ($\delta^2\text{H}$ and $\delta^{18}\text{O}$) technologies (see Williams et al.,
528 2004), canopy temperature using infrared thermometer and continuous within- and
529 above-canopy radiation using the four-component net radiometer (see Sauer et al.,
530 2007) are needed in the future studies.

531 The method, as implemented here, used all observations simultaneously to
532 constrain parameters and obtain an optimal match between data and model. After
533 parameter optimizing, the main source of model error can be attributed to the model
534 structure. Thus, this method facilitates the detection of the model structural failures.
535 Until now, numerous models, retaining the S-W model as basis, have been developed
536 for estimating ET or its different components, and they tended to be more and more
537 complex (see Lhomme et al., 2012). However, increasing model complexity is always
538 accompanied by a great danger of equifinality and large uncertainties in forward runs
539 (Beven et al., 1989; Franks and Beven, 1997). Most importantly, we must ensure that
540 we are on the right direction in modifying the model. In this study, we found that the
541 S-W model applied in arid areas generally failed when local advection occurred (Fig.

542 9). Thus, we thought that the main structural error of the S-W model as well as its
543 various extensions comes from the ignorance of the effects of advection on the ET
544 processes. A potential solution is to add the additional energy (negative H) to the
545 available energy term defined in equation 12 (see Parlange and Katul, 1992).

546 The distribution of the model-minus-observation residuals, through the
547 likelihood function, may also have an influence on the estimation of posterior
548 parameter distributions (Raupach et al., 2005). However, a *priori* assessment of these
549 errors may be not easy (Beven, 2001). Fig. 11 shows the distribution of the residuals
550 between simulated and observed datasets. The results indicated that the
551 model-minus-observation departures of half-hourly λ ET flux was better approximated
552 by a double-exponential distribution, which was in agreement with previous studies
553 (Hollinger and Richardson, 2005; Richardson et al., 2006). Thus, the two-tower
554 approach (Hollinger and Richardson, 2005), which can give a prior estimates of the
555 flux data uncertainties, should be applied in the Bayesian inference in future studies.
556 The Cauchy distribution gave a more appropriate approximation for the daily E
557 departures. However, the Cauchy distribution may be not a good choice for the
558 purpose of Bayesian inference, since its first four moments are undefined (Richardson
559 et al., 2008).

560 **5 Conclusions**

561 This study illustrated the use of the Bayesian method to simultaneously
562 parameterize a two-source ET model against the **multivariate datasets** for a crop
563 ecosystem in a desert oasis of northwest China. The posterior distributions of the

564 model parameters in most cases can be well constrained by the observations.
565 Generally, the parameterized model has a good performance in simulating and
566 partitioning ET. However, underestimations were observed on days when **the**
567 **'oasis-effect' occurred**. Therefore, in the future studies, special attentions should be
568 given to proper descriptions of the effects of advection on estimating ET for
569 heterogeneous land surface. In addition, the canopy interception model should be
570 coupled with the two-source ET model in long-term simulation.

571 *Acknowledgements*

572 The eddy covariance flux, meteorological, and other data used in this study are
573 from Heihe Watershed Allied Telemetry Experimental Research (HiWATER)
574 (<http://heihedata.org/hiwater>). We thank all the scientists, engineers and students who
575 participated in HiWATER field campaigns. This research was supported by National
576 Natural Science Foundation of China (No. 31370467), the Chinese Academy of
577 Sciences Action Plan for West Development Program Project (KZCX2-XB3-15), New
578 Century Excellent Talents in University of Chinese Ministry of Education (No.
579 NCET-11-0219), and the One Hundred Person Project of the Chinese Academy of
580 Sciences (No. 29Y127D01).

581 **References**

582 Allen, R.G., Pereira, L.S., Raes, D., Smith, M.: Crop evapotranspiration- guidelines
583 for computing crop water requirements. FAO Irrigation and Drainage Paper, No.
584 56, FAO, Rome, 1998.

585 Anadranistakis, M., Liakatas, A., Kerkides, P., Rizos, S., Gavanosis, J., Poulouvassilis,

586 A.: Crop water requirements model tested for crops grown in Greece. *Agr. Water*
587 *Manage.*, 45 (3), 297-316, 2000.

588 Bastola, S., Murphy, C., Sweeney, J.: The role of hydrological modelling uncertainties
589 in climate change impact assessments of Irish river catchments. *Adv. Water*
590 *Resour.*, 34, 562-576, 2011.

591 Beven, K.: Changing ideas in hydrology-The case of physically-based model. *J.*
592 *Hydrol.*, 105, 157-172, 1989.

593 Beven, K.: How far can we go in distributed hydrological modelling ? *Hydrol. Earth*
594 *Syst. Sci.*, 5(1), 1-12, 2001.

595 Beven, K.J., Smith, P.J., Freer, J.E.: So just why would a modeller choose to be
596 incoherent? *J. Hydrol.*, 354, 15-32, 2008.

597 Bouten, W., Schaap, M.G., Aerts, J., Vermetten, A.W.M.: Monitoring and modelling
598 canopy water storage amounts in support of atmospheric depositions studies. *J.*
599 *Hydrol.*, 181: 305-321, 1996.

600 Braswell, B., Sacks, W.J., Linder, E., Schimel, D.S.: Estimating diurnal to annual
601 ecosystem parameters by synthesis of a carbon flux model with eddy covariance
602 net ecosystem exchange observations. *Global Change Biol.*, 11, 1-21, 2005.

603 Brigode a, P., Oudin, L., Perrin, C.: Hydrological model parameter instability: A
604 source of additional uncertainty in estimating the hydrological impacts of climate
605 change? *J. Hydrol.*, 476, 410-425, 2013.

606 Clark, J.S., Gelfand, A.E.: A future for models and data in environmental science.
607 *Trends Ecol. Evol.*, 12, 375-380, 2006.

608 Daamen, C., Simmonds, L.E., Wallace, J.S., Laryea, K.B., Sivakumar, M.U.K.: Use
609 microlysimeters to measure evaporation from sandy soils. *Agric. For. Meteor.*, 65,
610 159-173, 1993.

611 Engeland, K., Braud, I., Gottschalk, L., Leblois, E.: Multi-objective regional
612 modeling. *J. Hydrol.*, 327, 339-35, 2006.

613 Evett, S.R., Kustas, W.P., Gowda, P.H., Anderson, M.A., Prueger, J.H., Howell, T.A.:
614 Overview of the Bushland Evapotranspiration and Agricultural Remote sensing
615 EXperiment 2008 (BEAREX08): A field experiment evaluating methods for
616 quantifying ET at multiple scales. *Adv. Water Resour.*, 50, 4-19, 2012.

617 Fenicia, F., Savenije, H.H.G., Matgen, P., Pfister, L.: A comparison of alternative
618 multiobjective calibration strategies for hydrological modeling. *Water Resour.*
619 *Res.*, 43, W03434, 2007.

620 Ferretti, D., Pendall, E., Morgan, J., Nelson, J., LeCain, D., Mosier, A.: Partitioning
621 evapotranspiration fluxes from a Colorado grassland using stable isotopes:
622 seasonal variations and ecosystem implications of elevated atmospheric CO₂.
623 *Plant and Soil*, 254(2), 291-303, 2003.

624 Flumignan, D.L., Faria, R.T., Prete, C.E.C.: Evapotranspiration components and dual
625 crop coefficients of coffee trees during crop production. *Agr. Water Manage.*, 98,
626 791-800, 2011.

627 Franks, S.W., Beven, K.J., Quinn, P.F., Wright, I.R.: On the sensitivity of
628 soil-vegetation-atmosphere transfer (SVAT) schemes: equifinality and the
629 problem of robust calibration. *Agric. For. Meteorol.*, 86, 63-75, 1997.

630 Franks, S.W., Beven, K.J.: Bayesian estimation of uncertainty in land
631 surface-atmosphere flux predictions. *J. Geophys. Res. Atmos.*, 102, 23991-23999,
632 1997.

633 Gash, J.H.C., Lloyd, C. R., Lachaud, G., Estimating sparse forest rainfall interception
634 with an analytical model. *J. Hydrol.*, 170, 79-86, 1995.

635 Gelman, A., Rubin, D.B. Inference from Iterative Simulation Using Multiple
636 Sequences. *Statistical Sciences*, 7, 457-511, 1992.

637 Gelman, A.B., Carlin, J.S., Stern, H.S. Rubin, D.B.: *Bayesian Data Analysis. Texts in*
638 *Stat. Sci. Ser.*, edited by C. Chatfield and J.V. Zidek, CRC Press, Boca Raton,
639 Florida, 1995.

640 Hanan, N.P., Prince, S.D.: Stomatal conductance of west-central supersite vegetation
641 in HAPEX-Sahel: measurements and empirical model. *J. Hydrol.*, 188-189,
642 536-562, 1997.

643 Harris, P.P., Huntingford, C., Cox, P.M., Gash, J.H.C., Malhi, Y.: Effect of soil
644 moisture on canopy conductance of Amazonian rainforest. *Agric. For. Meteor.*,
645 122, 215-227, 2004.

646 Hastings, W.K.: Monte Carlo sampling methods using Markov chains and their
647 applications. *Biometrika*, 57, 97-109, 1970.

648 Hollinger, D.Y., Richardson, A.D.: Uncertainty in eddy covariance measurements and
649 its application to physiological models. *Tree Physiol.*, 25, 873-885, 2005.

650 Hrachowitz, M., Savenije, H., Bogaard, T.A., Tetzlaff, D., Soulsby, C.: What can
651 flux tracking teach us about water age distribution patterns and their temporal

652 dynamics? *Hydrol. Earth Syst. Sci.*, 17, 533-564, 2013.

653 Hrachowitz, M., Savenije, H.H.G., Blöschl, G., McDonnell, J.J., Sivapalanf, M.,
654 Pomeroy, J.W., Arheimer, B., Blumei, T., Clark, M.P., Ehret, U., Feniciaal, F.,
655 Freer, J.E., Gelfann, A., Guptao, H.V., Hughes, D.A., Hut, R.W., Montanari, A.,
656 Pandeia, S., Tetzlaff, D., Trocho, P.A., Uhlenbrook, S., Wagener, T., Winsemius,
657 H.C., Woods, R.A., Zehek, E., Cudennec, C.: A decade of Predictions in
658 Ungauged Basins (PUB)- a review. *Hydrolog. Sci. J.*, 58(6), 1198-1255, 2013.

659 Hu, Y.Q.: Research advance about the energy budget and transportation of water
660 vapour in the HEIFE area. *Advance in Earth Science*, 9(4), 30-34, 1994. (in
661 Chinese with English abstract).

662 Hu, Z.M., Yu, G.R., Zhou, Y.L., Sun, X.M., Li, Y.N., Shi, P.L., Wang, Y.F., Song, X.,
663 Zheng, Z.M., Zhang, L., Li, S.G.: Partitioning of evapotranspiration and its
664 controls in four grassland ecosystems: Application of a two-source model. *Agric.*
665 *For. Meteor.*, 149, 1410-1420, 2009.

666 Iman, R.L., Helton, J.C.: An investigation of uncertainty and sensitivity analysis
667 techniques for computer models. *Risk Anal.*, 8(1), 71-90, 1988.

668 Jarvis, P.G.: The interpretation of the variations in leaf water potential and stomatal
669 conductance found in canopies in the field. *Philos. T. R. Soc. B.*, 273, 563-610,
670 1976.

671 Kato, T., Kimura, R., Kamichika, M.: Estimation of evapotranspiration, transpiration
672 ratio and water-use efficiency from a sparse canopy using a compartment model.
673 *Agr. Water Manage.*, 65 (3), 173-191, 2004.

674 Kavetski, D., Kuczera, G., Franks, S.W.: Bayesian analysis of input uncertainty in
675 hydrological modeling: 1. Theory. *Water Resour. Res.*, 42, W03407,
676 doi:10.1029/2005WR004368, 2006.

677 Knorr, W., Kattge, J.: Inversion of terrestrial ecosystem model parameter values
678 against eddy covariance measurements by Monte Carlo sampling. *Global Change*
679 *Biol.*, 11, 1333-1351, 2005.

680 Korner, C., Schecl, J.A., Bauer, H. Maximum leaf diffusive conductance in vascular
681 plants. *Photosynrherica*, 13, 45-82, 1979.

682 Legates, D.R., McCabe, G.J.: Evaluating the use of ‘goodness-of-fit’ measures in
683 hydrologic and hydroclimatic model validation. *Water Resour. Res.*, 35, 233-241,
684 1999.

685 Lemon, E.R., Glaser, A.H., Satterwhite, L.E.: Some aspects of the relationship of soil,
686 plant, and meteorological factors to evapotranspiration. *Proc. Soil Sci. Soc. Amer.*,
687 21, 464-468, 1957.

688 Lhomme, J.P., Montes, C., Jacob, F., Prévot, L.: Evaporation from Heterogeneous and
689 Sparse Canopies: On the Formulations Related to Multi-Source Representations.
690 *Boundary-Layer Meteorol.*, 144, 243–262, 2012.

691 Lhomme, J.P., Montes, C., Jacob, F., Prévot, L.: Evaporation from Heterogeneous and
692 Sparse Canopies: On the Formulations Related to Multi-Source Representations.
693 *Boundary-Layer Meteorol.*, 144, 243-262, 2012.

694 Li, S.E., Kang, S.Z., Zhang, L., Ortega-Farias, S., Li, F.S., Du, T.S., Tong, L., Wang,
695 S.F., Ingman, M., Guo, W.H.: Measuring and modeling maize evapotranspiration

696 under plastic film-mulching condition. *J. Hydrol.*, 503, 153-168, 2013a.

697 Li, X., Cheng, G.D., Liu, S.M., Xiao, Q., Ma, M.G., Jin, R., Che, T., Liu, Q.H., Wang,
698 W.Z., Qi, Y., Wen, J.G., Li, H.Y., Zhu, G.F., Guo, J.W., Ran, Y.H., Wang, S.G.,
699 Zhu, Z.L., Zhou, J., Hu, X.L., Xu, Z.W.: Heihe Watershed Allied Telemetry
700 Experimental Research (HiWATER): Scientific objectives and experimental
701 design1. *B. Am. Meteorol. Soc.*, 94(8), 1145-1160, 2013b.

702 Liu, C.M., Zhang, X.Y., Zhang, Y.Q.: Determination of daily evaporation and
703 evapotranspiration of winter wheat and maize by large-scale weighing lysimeter
704 and micro-lysimeter. *Agric. For. Meteorol.*, 111, 109-120, 2002.

705 Liu, S.M., Xu, Z.W., Wang, W.Z., Jia, Z.Z., Zhu, M.J., Bai, J., Wang, J.M.: A
706 comparison of eddy-covariance and large aperture scintillometer measurements
707 with respect to the energy balance closure problem. *Hydrol. Earth Syst. Sci.*, 15,
708 1291-1306, 2011.

709 Lund, M.R., Soegaard, H.: Modelling of evaporation in a sparse millet crop using a
710 two-source model including sensible heat advection within the canopy. *J. Hydrol.*,
711 280, 124-144, 2003.

712 Mann, J., Lenschow, D.H.: Errors in airborne flux measurements. *J. Geophys. Res.*,
713 99, 14519-14526, 1994.

714 Metropolis, N.R., Rosenbluth, A.W., Rosenbluth, M.N., Teller, A.H.: Equations of
715 state calculations by fast computing machines. *J. Chem. Phys.*, 21, 1087-1091,
716 1953.

717 Mo, X.G., Lin, Z.H., Xiang, Y.Q., Liu, S.X.: Characteristics of incoming radiation

718 through maize canopy. *Eco-agriculture Research*, 8, 1-4, 2000.

719 Morison, J.I.L., Baker, N.R., Mullineaux, P.M., Davies, W.J.: Improving water use in
720 crop production. *Phil. Trans. R. Soc. B.*, 363, 639-658, 2008.

721 **Moussa, R., Chahinian, N.: Comparison of different multi-objective calibration**
722 **criteria using a conceptual rainfall–runoff model of flood events. *Hydrol. Earth***
723 ***Syst. Sci.*, 13, 519-535, 2009.**

724 Mulder, J.P.M.: Simulating interception loss using standard meteorological data. *The*
725 *Forest-Atmosphere Interaction*, B. Hutchison and B. Hicks, Eds., D. Reidel,
726 177-196, 1985.

727 Noilhan, J., Planton, S.: A simple parameterization of land surface processes for
728 meteorological Models, *Mon. Weather Rev.*, 117, 536-549, 1989.

729 Ogink-Hendriks, M.J.: Modelling surface conductance and transpiration of an
730 oak forest in the Netherlands. *Agric. For. Meteorol.*, 74, 99-118, 1995.

731 **Oke, T. R.: *Boundary layer Climates. Second edn. Methuen, London, 1978.***

732 Ortega-Farias, S., Carrasco, M., Oliosio, A., Acevedo, C., Poblete, C.: Latent heat flux
733 over a Cabernet Sauvignon vineyard using the Shuttleworth and Wallace model.
734 *Irrig. Sci.*, 25, 161-170, 2007.

735 Ortega-Farias, S., Poblete-Echeverria, C., Brisson, N.: Parameterization of a two-layer
736 model for estimating vineyard evapotranspiration using meteorological
737 measurements. *Agric. For. Meteorol.*, 150, 276-286, 2010.

738 **Parlange, M.B., Katul, G.G.: An advection-aridity evaporation model. *Water Resour.***
739 ***Res.*, 28(1), 127-132, 1992.**

740 Poblete-Echeverria, C., Ortega-Farias, S.: Estimation of actual evapotranspiration for
741 a drip-irrigated Merlot vineyard using a three-source model. *Irrigation Sci.*, 28,
742 65-78, 2009.

743 Pospisilova, J., Solarova, J.: Environmental and biological control of diffusive
744 conductance of adaxial and abaxial leaf epidermis. *Photosyntherica*, 14, 90-127,
745 1980.

746 Rana, G., Katerji, N.: Measurement and estimation of actual evapotranspiration in
747 the field under Mediterranean climate: a review. *Eur. J. Agron.*, 13(2-3), 125-153,
748 2000.

749 Rao, K., Wyngaard, J., Cote, O.: Local advection of momentum, heat, and moisture in
750 micrometeorology. *Boundary-Layer Meteorol.*, 7(3), 331-348, 1974.

751 Raupach, M.R., Rayner, P.J., Barrett, D.J., Defries, R.S., Heimann, M., Ojima, D.S.,
752 Quegan, S., Schimullius, C.C.: Model-data synthesis in terrestrial carbon
753 observation: methods, data requirements and data uncertainty specifications.
754 *Global Change Biol.*, 11, 378-397, 2005.

755 Richardson, A.D., Hollinger, D.Y., Burba, G.G., Davis, K.J., Flanagan, L.B., Katul,
756 G.G., Williammunger, J., Ricciuto, D.M., Stoy, P.C., Suyker, A.E., Verma, S.B.,
757 Wofsy, S.C.: A multi-site analysis of random error in tower-based measurements
758 of carbon and energy fluxes. *Agric. For. Meteorol.*, 136, 1-18, 2006.

759 Richardson, A.D., Mahecha, M.D., Falge, E., Kattge, J., Moffat, A.M., Papale, D.,
760 Reichstein, M., Stauch, V.J., Braswell, B.H., Churkina, G., Kruijt, B., Hollinger,
761 D.Y.: Statistical properties of random CO₂ flux measurement uncertainty inferred

762 from model residuals. *Agric. For. Meteor.*, 148, 38-50, 2008.

763 Richardson, A.D., Williams, M., Hollinger, D.Y., Moore, D.J.P., Dail, D.B., Davidson,
764 E.A., Scott, N.A., Evans, R.S., Hughes, H., Lee, J.H., Rodrigues, C., Savage, K.:
765 Estimating parameters of a forest ecosystem C model with measurements of
766 stocks and fluxes as joint constraints. *Oecologia*, 164, 25-40, 2010.

767 Rutter, A.J., Kershaw, K. A., Robbins, P.C., Morton, A. J.: A predictive model of
768 rainfall interception in forests. I. Derivation of the model from observations in a
769 plantation of Corsican pine. *Agric. For. Meteor.*, 9, 367-384, 1971.

770 Samanta, S., Mackay, D.S., Clayton, M.K., Kruger, E.L., Ewers, B.E.: Bayesian
771 analysis for uncertainty estimation of a canopy transpiration model. *Water*
772 *Resour. Res.*, 43, W04424. <http://dx.doi.org/10.1029/2006WR005028>, 2007.

773 Sauer, T.J., Singer J.W., Prueger, J.H., DeSutter, T.M., Hatfield, J.L.: Radiation
774 balance and evaporation partitioning in a narrow-row soybean canopy. *Agric. For.*
775 *Meteor.*, 145, 206-214, 2007.

776 Scott, R.L., Huxman, T.E., Cable, W.L., Emmerich, W.E.: Partitioning of
777 evapotranspiration and its relation to carbon dioxide exchange in a Chihuahuan
778 desert shrubland. *Hydrol. Processes.*, 20, 3227-3243, 2006.

779 Sellers, P.J., Heiser, M.D., Hall, F.G.: Relations between surface conductance and
780 spectral vegetation indices at intermediate (100 m² to 15 km²) length scales. *J.*
781 *Geophys. Res.*, 97 (D17), 19033-19059, 1992.

782 Shuttleworth, W.J., Gurney, R.J.: The theoretical relationship between foliage
783 temperature and canopy resistance in sparse crops. *Q. J. Roy. Meteor. Soc.*, 116,

784 497-519, 1990.

785 Shuttleworth, W.J., Wallace, J.S.: Evaporation from sparse crops- an energy
786 combination theory. *Q. J. Roy. Meteor. Soc.*, 111, 839-855, 1985.

787 Stannard, D.I.: Comparison of Penman-Monteith, Shuttleworth-Wallace and modified
788 Priestley-Taylor evapotranspiration models for wildland vegetation in semiarid
789 rangeland. *Water Resour. Res.*, 29, 1379-1392, 1993.

790 Stewart, J.B.: Modelling surface conductance of pine forest. *Agric. For. Meteor.*, 43,
791 19-35, 1988.

792 Sun, H.Y., Shao, L.W., Liu, X.W., Miao, W.F., Chen, S.Y., Zhang, X.Y.:
793 Determination of water consumption and the water-saving potential of three
794 mulching methods in a jujube orchard. *Eur. J. Agron.*, 43, 87-95, 2012.

795 Sun, S.F.: Moisture and heat transport in a soil layer forced by atmospheric conditions.
796 M.S. thesis, University of Connecticut, 1982.

797 Svensson, M., Jansson, P.E., Gustafson, D., Kleja, D.B., Langvall O., Lindroth, A.:
798 Bayesian calibration of a model describing carbon, water and heat fluxes for a
799 Swedish boreal forest stand. *Ecol. Model.*, 213, 331-344, 2008..

800 Teh, C.B.S., Simmonds, L.P., Wheeler, T.R.: Modelling the partitioning of solar
801 radiation capture and evapotranspiration intercropping systems. In: Proceedings
802 of the 2nd International Conference on Tropical Climatology, Meteorology and
803 Hydrology TCMH-2001, Brussels, Belgium, 2001.

804 Tourula, T., Heikinheimo, M.: Modelling evapotranspiration from a barley field over
805 the growing season. *Agric. For. Meteor.*, 91(3-4), 237-250, 1998.

806 United Nations Environment Programme (UNEP): World Atlas of Desertification.
807 London. Edward Arnold, 1992.

808 van de Griend, A.A., Owe, M.: Bare soil surface resistance to evaporation by vapor
809 diffusion under semiarid conditions. *Water Resour. Res.*, 30 (2), 181-188, 1994.

810 van Oijen, M., Cameron, D.R., Butterbach-Bahl, K., Farahbakhshazad, N., Jansson,
811 P.E., Kiese, R., Rahn, K.H., Werner, C., Yeluripati, J.B.: A Bayesian framework
812 for model calibration, comparison and analysis: application to four models for the
813 biogeochemistry of a Norway spruce forest. *Agric. For. Meteorol.*, 151(12),
814 1609-1621, 2011.

815 van Oijen, M., Reyer, C., Bohn, F.J., Cameron, D.R., Deckmyn, G., Flechsig, M.,
816 Härkönen, S., Hartig, F., Huth, A., Kiviste, A., Lasch, P., Mäkelä, A., Mette, T.,
817 Minunno, F., Rammer, W.: Bayesian calibration, comparison and averaging of
818 six forest models, using data from Scots pine stands across Europe. *Forest Ecol.
819 Manag.*, 289, 255-268, 2013.

820 van Oijen, M., Rougier, J., Smith, R.: Bayesian calibration of process-based forest
821 models: bridging the gap between models and data. *Tree Physiol.*, 25(7), 915-927,
822 2005.

823 Verhoef, A., Allen, S.J.: A SVAT scheme describing energy and CO₂ fluxes for
824 multi-component vegetation: calibration and test for a Sahelian savannah. *Ecol.
825 Model.*, 127, 245–267, 2000.

826 Verhoef, A., Fernández-Gálvez, J., Diaz-Espejo, A., Main, B.E., El-Bishti, M. The
827 diurnal course of soil moisture as measured by various dielectric sensors: effects

828 of soil temperature and the implications for evaporation estimates. *J. Hydrol.*, 321,
829 147-162, 2006.

830 Verhoef, A., Otle, C., Cappelaere, B., Murray, T., Saux-Picart, S., Zribi, M., Maignan,
831 F., Boulain, N., Demarty, J., Ramier, D.: Spatio-temporal surface soil heat flux
832 estimates from satellite data: results for the AMMA experiment at the Fakara
833 (Niger) supersite. *Agric. For. Meteorol.*, 154-155, 55-66, 2012.

834 Villagarcía, L., Were, A., García, M., Domingo, F.: Sensitivity of a clumped model of
835 evapotranspiration to surface resistance parameterisations: Application in a
836 semi-arid environment. *Agric. For. Meteorol.*, 150, 1065-1078, 2010.

837 Wallace, J.S., Verhoef, A.: Interactions in mixed-plant communities: light, water and
838 carbon dioxide. In: Marshall B, Roberts JA (eds) *Leaf development and canopy
839 growth*. Sheffield biological science series. Sheffield Academic Press, Sheffield,
840 204-250 pp., 2000.

841 Wang, J.M., Mitsuta, Y.: Evaporation from the desert: some preliminary results of
842 HEIFI. *Boundary-Layer Meteorol.*, 59, 413-418, 1992.

843 Wang, J.M., Zhuang, J.X., Wang, W.Z., Liu, S.M., Xu, Z.W.: Assessment of
844 Uncertainties in Eddy Covariance Flux Measurement Based on Intensive Flux
845 Matrix of HiWATER-MUSOEXE. *IEEE Geosciences and Remote Sensing
846 Letters*, 2014, (under review).

847 Wang, X.F., Yakir, D.: Using stable isotopes of water in evapotranspiration studies.
848 *Hydrol. Process.*, 14, 1407-1421, 2000.

849 Wang, Y.P., Leuning, R., Cleugh, H.A., Coppin, P.A.: Parameter estimation in surface

850 exchange models using nonlinear inversion: how many parameters can we
851 estimate and which measurements are most useful? *Glob. Chang. Biol.*, 7,
852 495-510, 2001.

853 Williams, D.G., Cable, W., Hultine, K., Hoedjes, J.C.B., Yezzer, E.A., Simonneau, V.,
854 Er-Raki, S., Boulet, G., de Bruin, H.A.R., Chehbouni, A., Hartogensis, O.K.,
855 Timouk, F.: Evapotranspiration components determined by stable isotope, sap
856 flow and eddy covariance techniques. *Agric. For. Meteorol.*, 125 (3-4), 241-258,
857 2004.

858 Winsemius, H.C., Savenije, H.H.G., Gerrits, A.M.J., Zapreeva, E.A., Klees, R.:
859 Comparison of two model approaches in the Zambezi river basin with regard to
860 model reliability and identifiability. *Hydrol. Earth Syst. Sci.*, 10, 339-352, 2006.

861 Xu, Z.W., Liu, S.M., Li, X., Shi, S.J., Wang, J.M., Zhu, Z.L., Xu, T.R., Wang, W.Z.,
862 Ma, M.G.: Intercomparison of surface energy flux measurement systems used
863 during the HiWATER-USOEXE. *J. Geophys. Res.*, 118, 13140-13157, 2014.

864 Zhang, B.Z., Kang, S.Z., Li, F.S., Zhang, L.: Comparison of three evapotranspiration
865 models to Bowen ratio-energy balance method for a vineyard in an arid desert
866 region of northwest China. *Agric. For. Meteorol.*, 148, 1629-1640, 2008.

867 Zhang, Q., Huang, R.H.: Water vapor exchange between soil and atmosphere over a
868 Gobi surface near an oasis in Summer. *Journal of Applied Meteorology*, 43(12):
869 1917-1928, 2004.

870 Zhang, X.: Improvement of a Soil-Atmosphere-Transfer Model for the Simulation
871 of Bare Soil Surface Energy Balances in Semiarid Areas. *Asia-Pacific J. Atmos.*

872 Sci., 48(1), 97-105, 2012.

873 Zhao, W.Z., Ji, X.B., Kang, E.S., Zhang, Z.H., Jin, B.W.: Evaluation of
874 Penman-Monteith model applied to a maize field in the arid area of northwest
875 China. *Hydrol. Earth Syst. Sci.*, 14, 1353-1364, 2010.

876 Zhu, G.F., Li, X., Su, Y.H., Lu, L., Huang, C.L.: Seasonal fluctuations and temperature
877 dependence in photosynthetic parameters and stomatal conductance at the leaf
878 scale of *Populus euphratica Oliv.* *Tree Physiol.*, 31(2), 178-195, 2011.

879 Zhu, G.F., Li, Z.Z., Su, Y.H., Ma, J.Z., Zhang, Y.Y.: Hydrogeochemical and isotope
880 evidence of groundwater evolution and recharge in Minqin Basin, Northwest
881 China. *J. Hydrol.*, 333, 239-251, 2007.

882 Zhu, G.F., Su, Y.H., Feng, Q.: The Hydrochemical Characteristics and Evolution of
883 Groundwater and Surface Water in the Heihe River Basin, Northwest China.
884 *Hydrogeol. J.*, 16, 167-182, 2008.

885 Zhu, G.F., Su, Y.H., Li, X., Zhang, K., Li, C.B.: Estimating actual evapotranspiration
886 from an alpine grassland on Qinghai-Tibetan plateau using a two-source model
887 and parameter uncertainty analysis by Bayesian approach. *J. Hydrol.*, 476, 42-51,
888 2013.

889

890

891

892

893

894 **Figure Lists:**

895 **Fig. 1** Experimental location and instrumentation setting at Daman (DM) superstation.

896 **Fig. 2** Schematic diagram of the S-W model. From right to left, r_s^c and r_a^c are bulk
897 resistances of canopy stomatal and boundary layer ($s\ m^{-1}$), respectively; r_a^s and r_a^a
898 aerodynamic resistances from soil to canopy and from canopy to reference height (s
899 m^{-1}), respectively; r_s^s soil surface resistance ($s\ m^{-1}$). λT transpiration from canopy
900 ($W\ m^{-2}$), λE evaporation from soil under plant ($W\ m^{-2}$), and λET total
901 evapotranspiration ($W\ m^{-2}$).

902 **Fig. 3** Seasonal variation in (a) net solar radiation (R_n ; $MJ\ m^{-2}\ d^{-1}$), (b) air
903 temperature (T_a ; $^{\circ}C$), (c) vapor pressure deficit (D ; kPa), (d) wind speed (u ; $m\ s^{-1}$) at
904 the height of 3 m, (e) precipitation and irrigation (mm), soil water content (θ , $m^3\ m^{-3}$)
905 at 4, 10 20 and 40 cm depth, and (f) leaf are index (LAI; $m^2\ m^{-2}$) during the study
906 period in the Daman Oasis.

907 **Fig. 4** Histograms of samples from the posterior distributions of the parameters. The
908 dashed vertical lines indicate **median** parameter values.

909 **Fig. 5** Relative uncertainty reductions in the length of 95% credible interval form
910 prior to posterior distribution.

911 **Fig. 6** Comparisons of responses of soil surface resistance (r_s^s $s\ m^{-1}$) to soil surface
912 water contents (θ ; %).

913 **Fig. 7** (a) Plot of estimated evapotranspiration (λET ; $W\ m^{-2}$) against observed values.
914 The regressions is: $y = 0.84x + 0.18$ ($R^2 = 0.83$); (b) Plot of estimated daily soil
915 evaporation (E ; $mm\ d^{-1}$) against measured data. The regressions is: $y = 1.01x + 0.01$

916 ($R^2 = 0.82$).

917 **Fig. 8** Seasonal variation in daily evapotranspiration (ET; mm d^{-1}) and soil
918 evaporation (E ; mm day^{-1}) measured by the EC system and modeled by the S-W
919 model during the study period in Daman Oasis. Gap in the time series is caused either
920 by the absence of flux measurements or missing ancillary data.

921 **Fig. 9** Diurnal variations in net radiation flux (R_n ; W m^{-2}), sensible heat flux (H ; W m^{-2}),
922 and modeled and measured evapotranspiration flux (λET ; W m^{-2}). (a)-(c)
923 represented conditions at which micro-scale advection occurred at 12:00, 15:00 and
924 17:00 Beijing Standard Time (BST) , respectively, (d) represented a rainy day, and
925 (e)-(h) represented clear and advection-absent days during the study period. Gap is
926 caused either by the absence of flux measurements or missing ancillary data. **Modeled**
927 λET was presented as median $\pm 95\%$ posterior predication intervals.

928 **Fig. 10** The diurnal evolutions of temperature (T_a ; $^{\circ}\text{C}$) and relative humidity (RH; %)
929 profiles from 3 m to 40 m above the ground. (a) on 5 Jul. 2013. An obvious advection
930 process can be detected from 13:00 to 17:00 BST with high temperature and low RH
931 layer at the height of 8-18 m; (b) on 17 Jun. 2013. A precipitation event occurred at
932 13:00 and resulted in uniform vertical distributions of T_a and RH, but no temperature
933 inversion were observed; (c) on 11 Jun. 2013. It represented a typical clear and
934 advection-absent day.

935 **Fig. 11** Histograms depicting the frequency distribution of the
936 model-minus-observation departures for (a) half-hourly λET (W m^{-2}) and (b) daily
937 soil evaporation E (mm day^{-1}).

938 **Table 1** Prior distributions and the parameter bounds for the S-W model. These values are derived from the literature; The posterior parameter distribution estimated
 939 by MCMC are based on observed data in our site, and are characterized by the mean and 95% high-probability intervals (Lower limit, Upper limit).
 940

Parameter	Prior Distribution		References	Posterior Distribution	
	Lower Bound	Upper Bound		Median	95% High-Probability Interval
r_{STmin} (s m ⁻¹)	0	80	Noilhan and Planton (1989); Li et al. (2013a)	21.8	(20.2, 24.6)
k_1 (W m ⁻²)	0	500	Stewart (1998)	294.6	(42.5, 487.7)
k_2 (°C)	5	40	Ogink-Hendriks (1995)	25.6	(12.9,34.4)
k_3 (kPa ⁻¹)	0	0.1	Stewart (1998)	0.02	(0, 0.07)
b_1 (s m ⁻¹)	4	15	Sellers et al. (1992); Zhang (2012); Zhu et al., (2013)	9.3	(8.4, 10.0)
b_2 (s m ⁻¹)	0	8	Sellers et al. (1992); Zhang (2012) ; Zhu et al., (2013)	6.2	(3.8, 7.4)

941 The bold number means that this parameter was well constrained by the data.

942

943

944

945

946

947

948

949 **Table 2** Statistical analysis of measured and estimated **using the median parameter values** half-hourly evapotranspiration (λET ; $W m^{-2}$), daily soil evaporation (E ;
 950 $mm d^{-1}$), and daily evapotranspiration(ET ; $mm d^{-1}$) for the spring maize in arid desert oasis during the study period.

	n	Regressive equation	R^2	Mean measured values	Mean simulated values	RMSE	MBE	IA	EF
λET ($W m^{-2}$)	3578	$\lambda ET_{modeled}=0.84\lambda ET_{measured}+0.18$	0.83	161.4	137.2	80.7	24.2	0.93	0.74
E ($mm d^{-1}$)	56	$E_{modeled}=1.01E_{measured} +0.01$	0.82	0.26	0.28	0.05	-0.01	0.94	0.76
ET ($mm d^{-1}$)	95	$ET_{modeled}=0.83ET_{measured} +0.19$	0.83	2.02	1.88	0.32	0.14	0.94	0.79

951 n =the sample number; R^2 =the determination coefficient; RMSE=root mean square error; MBE=mean bias error between measured and modeled values; IA= index
 952 of agreement; ET= model efficiency. These statistical parameters are calculated using formulas given by Legates and McCabe (1999) and Poblete-Echeverria and
 953 Ortega-Farias (2009).

954

955

956

957

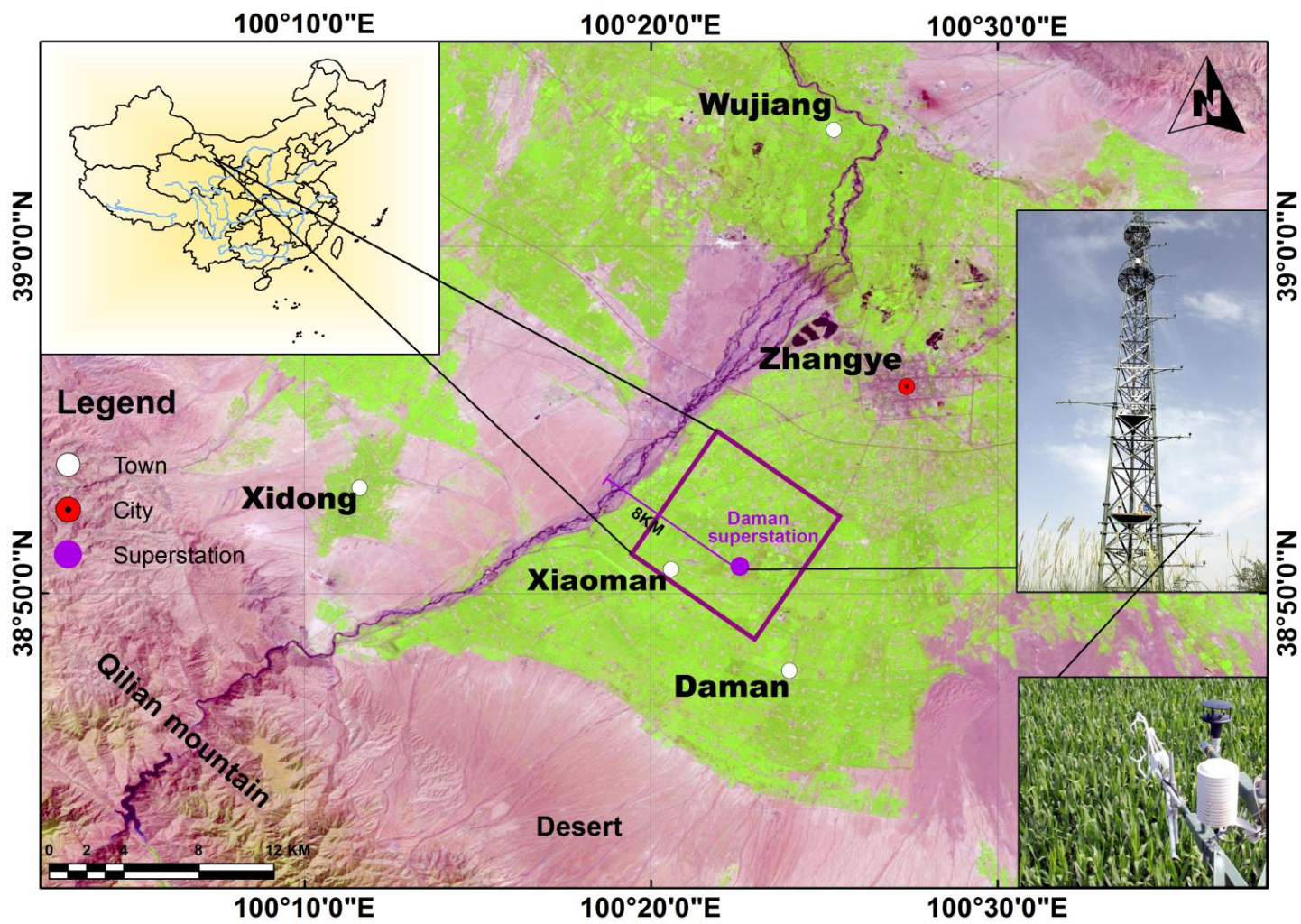
958

959

960

961

962



963

964

Fig. 1

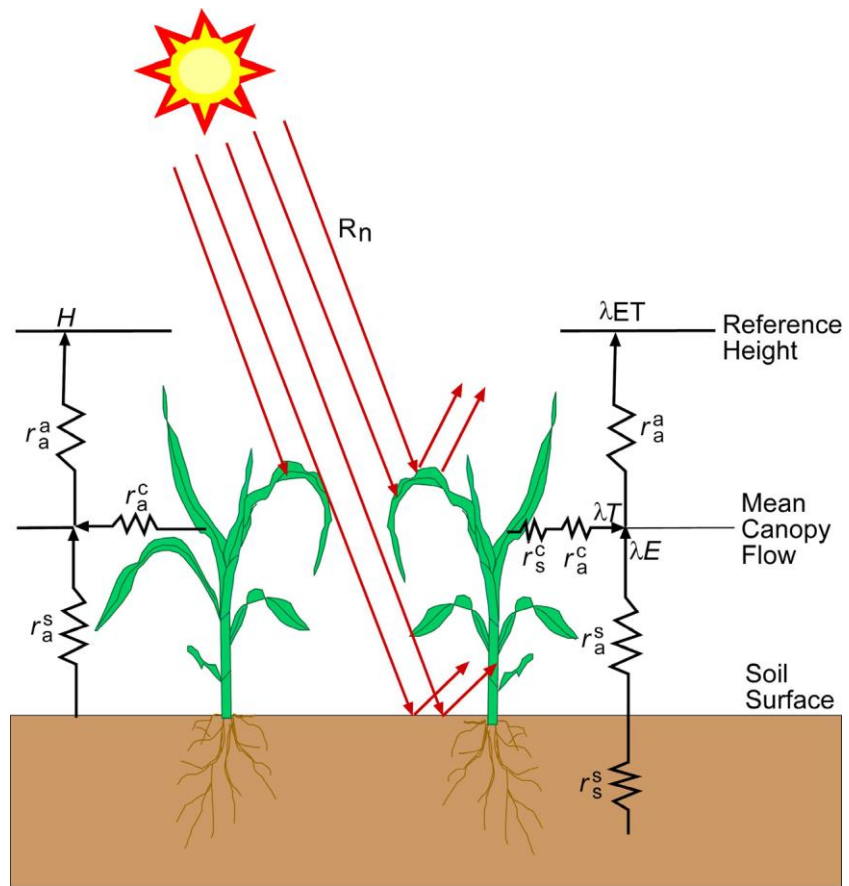


Fig. 2

965

966

967

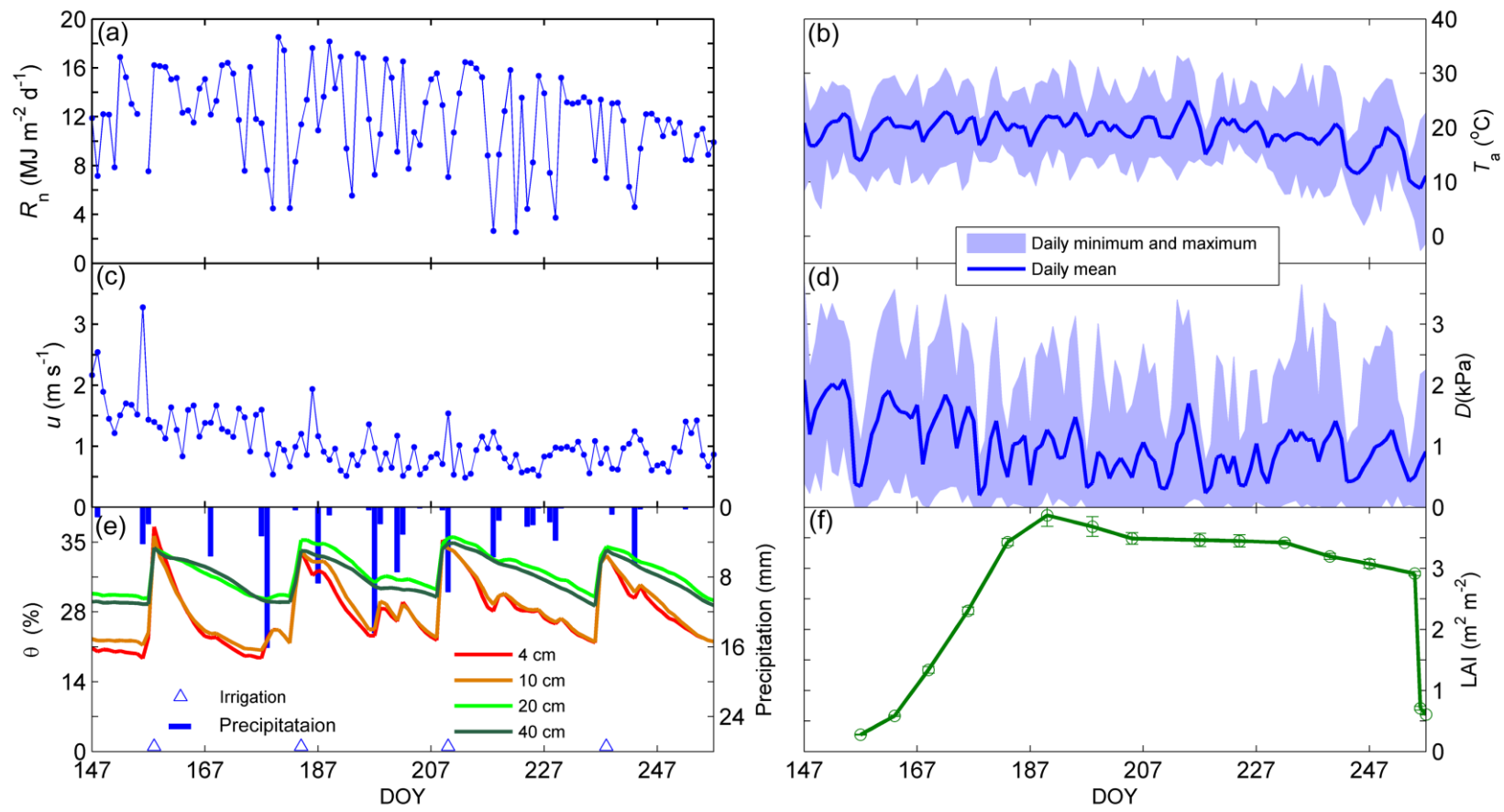


Fig. 3

968

969

970

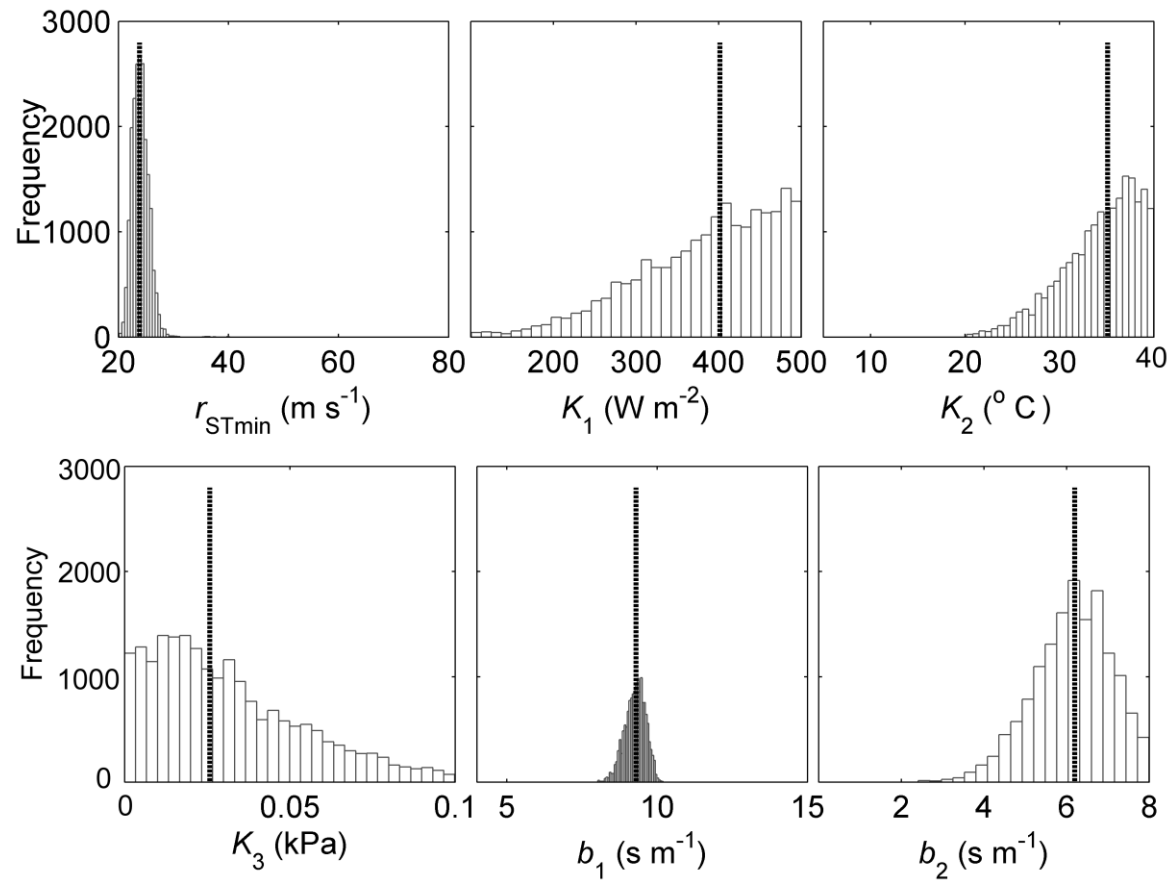


Fig. 4

971

972

973

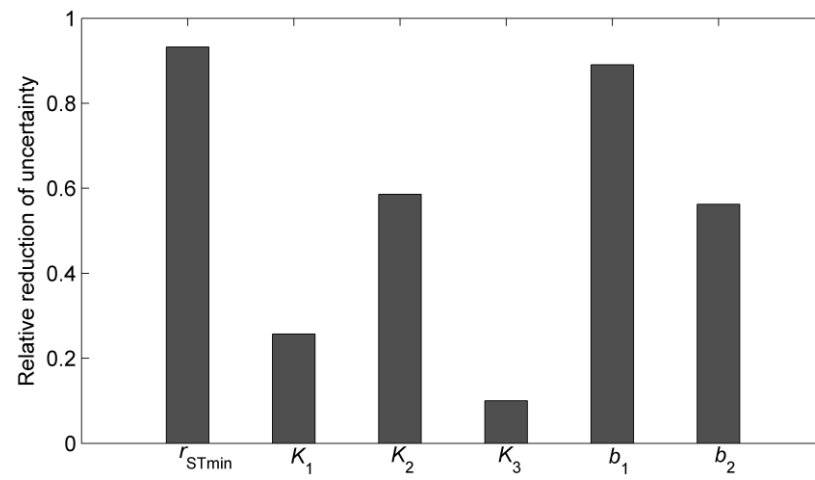


Fig. 5

974

975

976

977

978

979

980

981

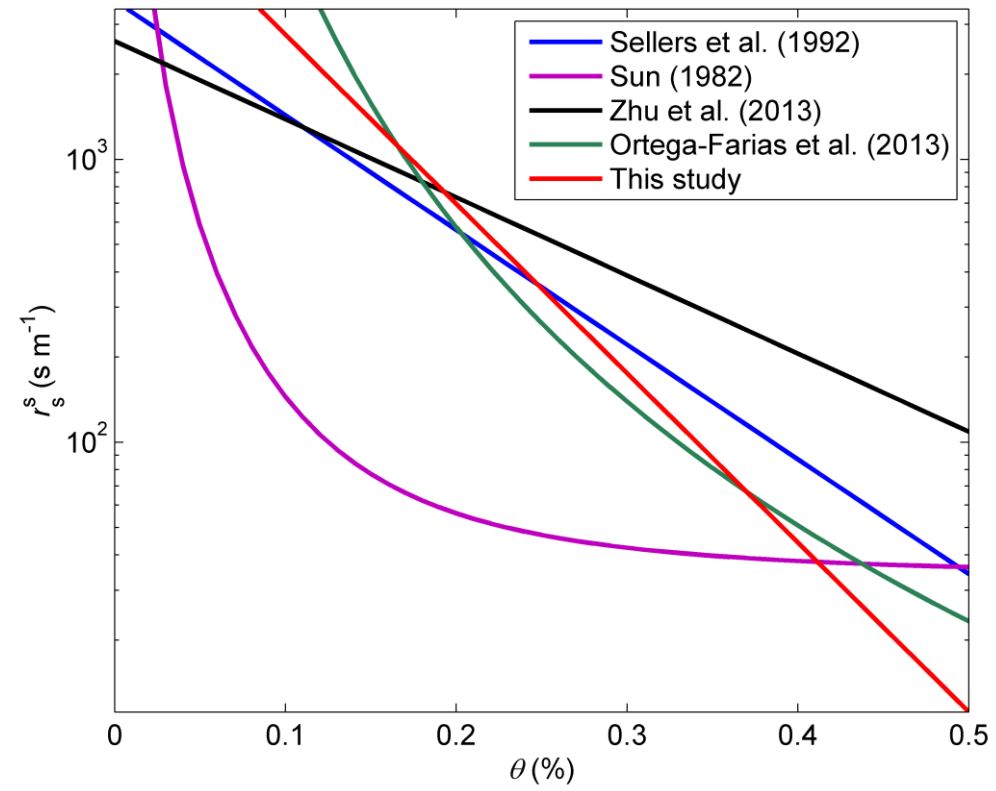


Fig. 6

982

983

984

985

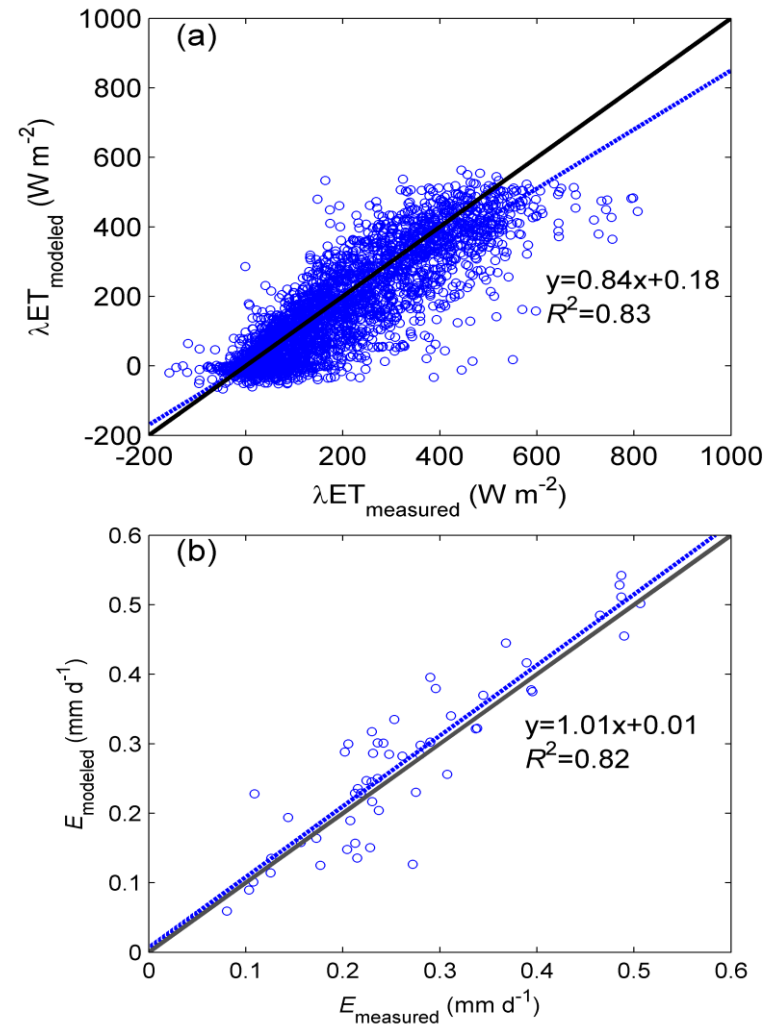


Fig. 7

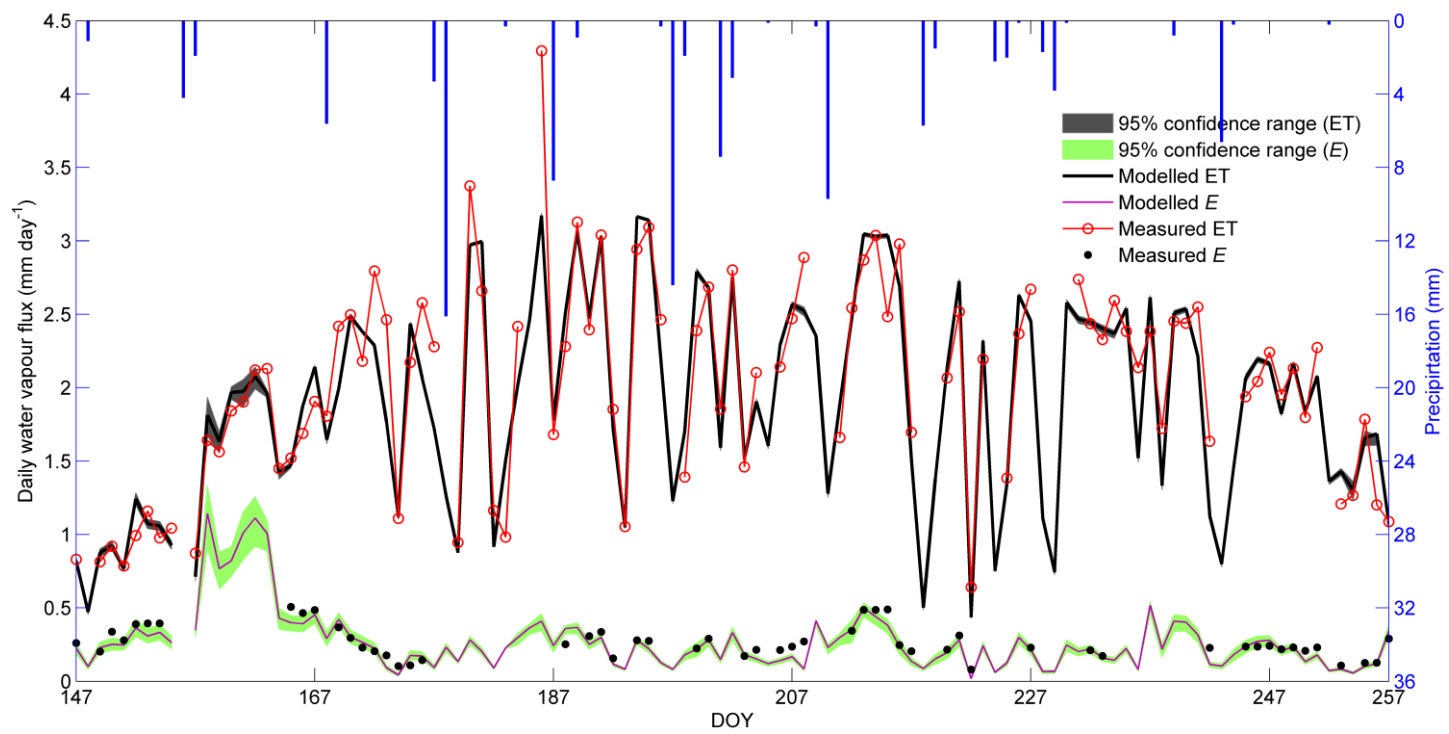


Fig. 8

988

989

990

991

992

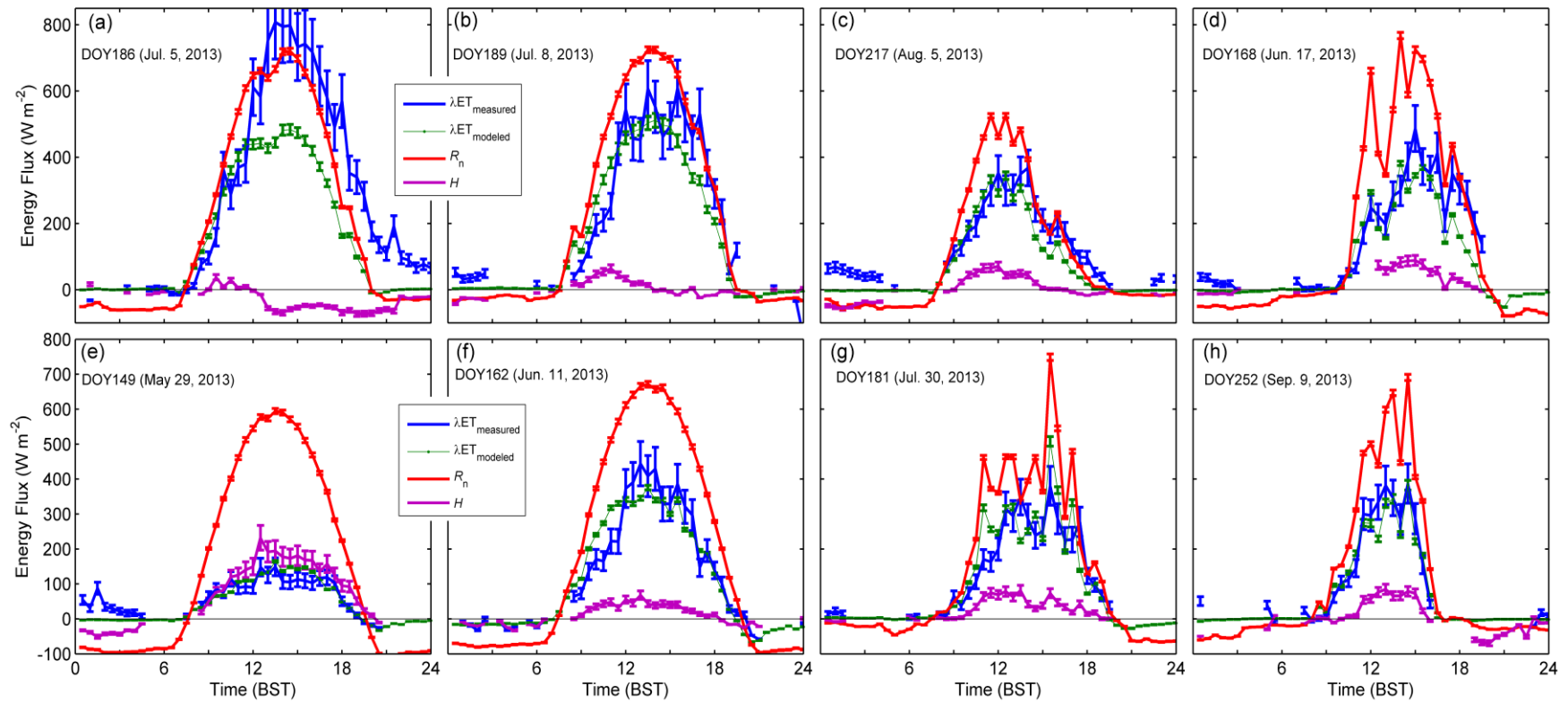


Fig. 9

993

994

995

996

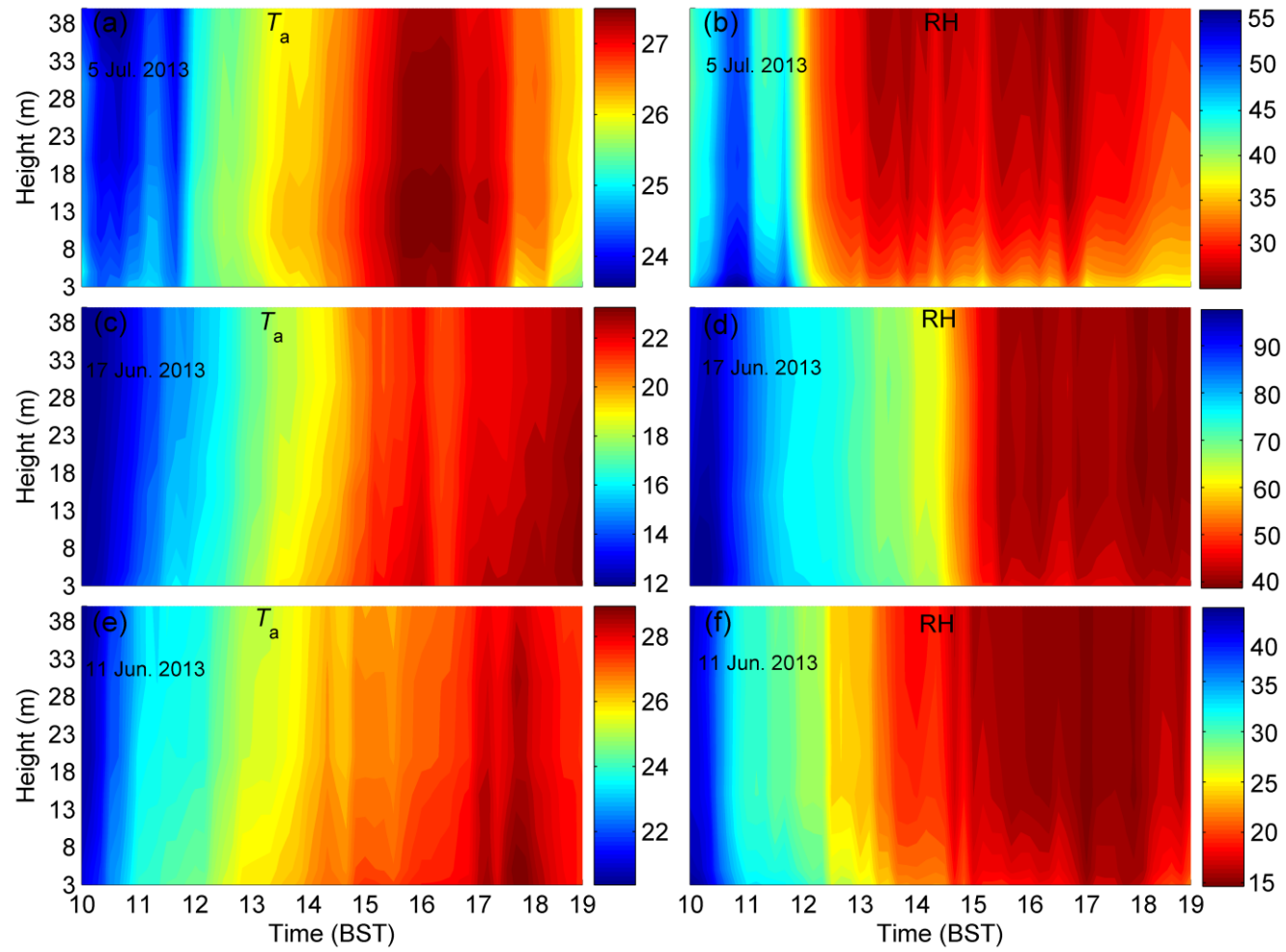


Fig. 10

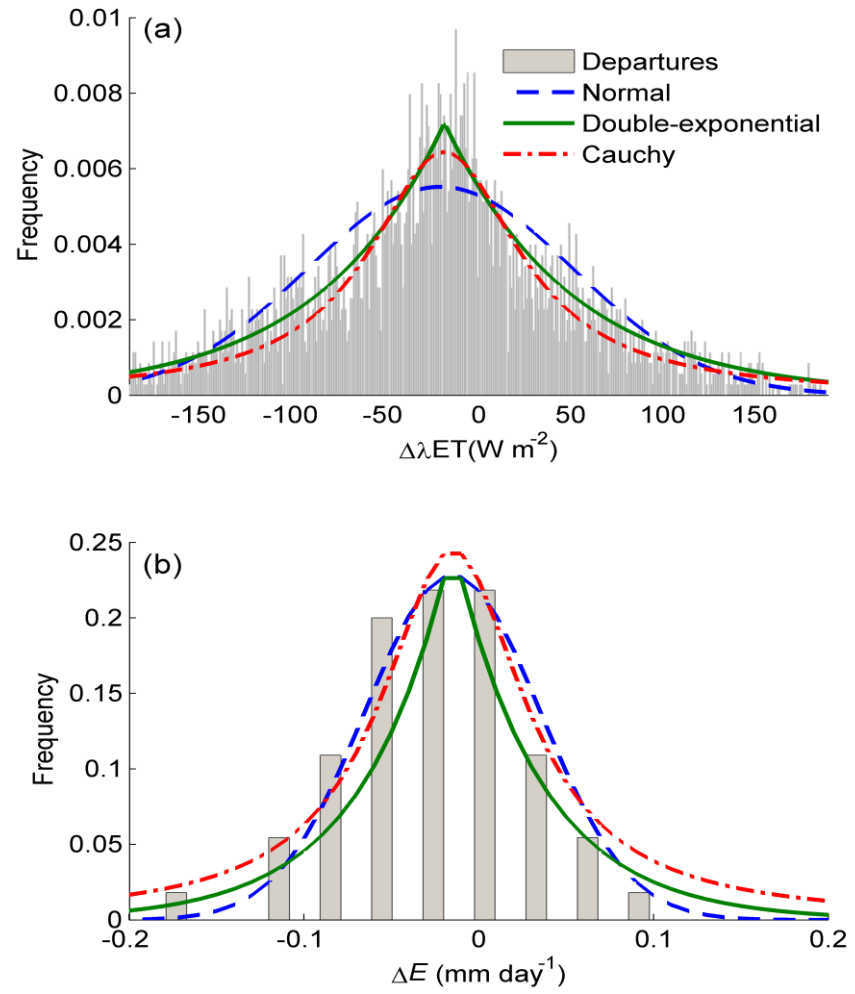


Fig. 11